UC Berkeley
UC Berkeley Previously Published Works

Title

Complementary first and second derivative methods for ansatz optimization in variational Monte Carlo

Permalink

https://escholarship.org/uc/item/2rh6w67x

Journal

Physical Chemistry Chemical Physics, 21(27)

ISSN

Authors

Otis, Leon
Neuscamman, Eric

Publication Date

2019-07-10

DOI

Peer reviewed

Complementary First and Second Derivative Methods for Ansatz Optimization in Variational Monte Carlo

Leon Otis[1] and Eric Neuscamman[2,3,*]

[1]*Department of Physics, University of California, Berkeley, CA, 94720, USA*
[2]*Department of Chemistry, University of California, Berkeley, CA, 94720, USA*
[3]*Chemical Sciences Division, Lawrence Berkeley National Laboratory, Berkeley, CA, 94720, USA*
(Dated: April 24, 2019)

We present a comparison between a number of recently introduced low-memory wave function optimization methods for variational Monte Carlo in which we find that first and second derivative methods possess strongly complementary relative advantages. While we find that low-memory variants of the linear method are vastly more efficient at bringing wave functions with disparate types of nonlinear parameters to the vicinity of the energy minimum, accelerated descent approaches are then able to locate the precise minimum with less bias and lower statistical uncertainty. By constructing a simple hybrid approach that combines these methodologies, we show that all of these advantages can be had at once when simultaneously optimizing large determinant expansions, molecular orbital shapes, traditional Jastrow correlation factors, and more nonlinear many-electron Jastrow factors.

INTRODUCTION

The practical utility of widely used methods in electronic structure theory is in large part determined by the optimization algorithms they rely on. This basic theme has been repeated throughout the history of quantum chemistry, with methods as fundamental as Hartree-Fock theory becoming dramatically more useful with the development of superior solution methods such as the direct inversion of the iterative subspace. [1] Similar transformations have been seen in configuration interaction (CI) theory thanks to Davidson's method, [2] in the density matrix renormalization group (DMRG) approach thanks to (among other innovations) the noise algorithm, [3] and in many other methods besides. As in the case of DMRG, it is usually not so simple as a single innovation in the numerical methods that transforms a theory from a promising proof of concept into a robust computational tool. Instead, such tools often arise as the result of a series of innovations, that, once combined, fit together in a way that makes them more than the sum of their parts.

In the context of quantum Monte Carlo (QMC), and more specifically in its variational (VMC) formulation, the introduction of the linear method (LM) for trial function optimization marked a large step forward along the path to practical utility and reliability. [4] However, recent research has revealed multiple options for bypassing the LM's memory bottleneck, making clear that there is still a great deal of distance to cover in the maturation of VMC numerical methods. Some of these approaches [5, 6] depend, like the LM itself, on knowing at least some information about energy second derivatives, but by avoiding the construction of full Hessian-sized matrices they achieve dramatically lower memory footprints compared to the LM. Other even more recent approaches, most of which can be classified as accelerated descent (AD) methods, [7–9] avoid second derivative information en-

tirely and are thus even more memory efficient, relying instead on a limited knowledge of the optimization's history of energy first derivatives or in one case just the signs of these derivatives. [10] In the present study, we explore the relative advantages of these first and second derivative approaches and find that, when combined, they offer a highly complementary optimization strategy that appears both more robust and more efficient than either class of methods is on its own.

The ability to optimize larger and more complicated wave function forms is becoming increasingly relevant due to rapid progress in other areas of VMC methodology. The introduction of the table method [11, 12] has increased the size of CI expansions that can be handled by more than an order of magnitude, and expansion lengths beyond 10,000 determinants are no longer unusual. A recent improvement to the table method [13, 14] now allows the molecular orbital basis to be optimized efficiently in the presence of these large expansions, while the resurgence of interest in selected CI methods [15–20] has provided a convenient route to their construction. In addition to these CI-based advances, other wave function innovations have also led to growing demands on VMC optimization methods. Increasingly sophisticated correlation factors, such as those used in Hilbert space approaches [5, 7–9, 21–23] as well as a steady stream of developments in real space [24–29] have also raised the demand for optimization approaches that can deal with large numbers of highly nonlinear parameters. Although less thoroughly explored, the treatment of correlation effects via back flow transformations also continues to receive attention and create new optimization challenges. [10, 30] Finally, in addition to these increases in ansatz sophistication, recent interest in using excited state variational principles to expand QMC's excited state capabilities has led to its own collection of optimization difficulties. [31–37]

By supporting these various advances in QMC methodology, improved VMC optimization methods have the potential for large impacts in diverse areas of chemistry and solid state physics. Work on lattice models, for example, continues to push the boundaries on how approximate wave functions are defined. [38, 39] In the area of molecular excited states, QMC methods offer promising new routes to high-accuracy treatments of both double excitations [31, 40] and charge transfer excitations, [33, 37] both of which continue to challenge conventional quantum chemistry methods. In QMC's traditional area of simulating real solids, applications of both VMC and projector Monte Carlo would benefit immediately from the ability to prepare more sophisticated trial wave functions. [41–43] Diffusion Monte Carlo (DMC) in particular would achieve higher accuracy using the better nodal surfaces determined by well-optimized ansatzes from VMC. More generally, the ability of QMC to combine treatments of weak and strong electron correlation effects within a robust variational framework that operates near the basis set limit makes it a powerful general-purpose approach for difficult molecular and materials problems where high accuracy is necessary. By increasing the size and complexity of systems that fall into its purview, improvements in QMC wave function optimization methods therefore have the potential to move electronic structure simulation forward on a number of fronts.

The present study seeks to aid in this endeavor by focusing on the relative advantages of recently developed low-memory first and second derivative methods in VMC and in particular on how they can be used to complement each other. Unlike deterministic optimizations, in which second derivative methods are typically preferred so long as they are affordable, the situation is less straightforward when the objective function and its derivatives are statistically uncertain. One major concern is that, in practice, it can be more difficult to achieve low-uncertainty estimates of the second derivative terms that appear in the LM and its descendants. While this issue can be mitigated by the use of alternative approaches to importance sampling, these can increase uncertainty in the energy due to the loss of the zero-variance principle. Thus, as we will demonstrate, statistical precision tends to be higher when using AD methods, which is an advantage on top of their ability to converge to the minimum without the bias that arises from the LM's highly nonlinear matrix diagonalization. However, we will also see that in order to enjoy the advantages of a tighter and less biased final convergence, AD methods must first reach the vicinity of the minimum. For this task, we find that the LM and its low-memory variants outperform all of the first derivative methods that we tested, especially for optimizations in which the wave function contains different classes of parameters that vary greatly in their nonlinear character and how they couple to each other. Happily, we will see that a hybrid approach — in

which AD and low-memory LM optimization steps are interwoven — excels both at reaching the vicinity of the minimum and producing unbiased final energies while simultaneously maintaining a high degree of statistical efficiency.

THEORY

Variational Monte Carlo

VMC combines the variational principle of quantum mechanics with Monte Carlo evaluation of high dimensional integrals.[44] To study the ground state of a system, we pick a trial wave function Ψ of some particular form and seek to minimize its energy expectation value.

$$E(\Psi) = \frac{\langle \Psi \mid H \mid \Psi \rangle}{\langle \Psi \mid \Psi \rangle} \qquad (1)$$

In the language of mathematical optimization, $E(\Psi)$ is an example of an objective function or cost function. For a typical system with N electrons, this expression contains integrals over $3N$ position space coordinates which for some wave functions can only be evaluated efficiently through Monte Carlo sampling rather than quadrature methods. We rewrite the energy as

$$E = \frac{\int d\mathbf{R}\Psi(\mathbf{R})H\Psi(\mathbf{R})}{\int d\mathbf{R}\Psi(\mathbf{R})^2} = \frac{\int d\mathbf{R}\Psi(\mathbf{R})^2 E_L(\mathbf{R})}{\int d\mathbf{R}\Psi(\mathbf{R})^2}$$
$$= \int d\mathbf{R}\rho(\mathbf{R})E_L(\mathbf{R}) \qquad (2)$$

where $E_L(\mathbf{R}) = \frac{H\Psi(\mathbf{R})}{\Psi(\mathbf{R})}$ is the local energy and $\rho(\mathbf{R}) = \frac{\Psi(\mathbf{R})^2}{\int d\mathbf{R}\Psi(\mathbf{R})^2}$ is the probability density. The zero-variance principle[45] makes $\rho(\mathbf{R})$ the most common choice of probability distribution for obtaining samples, but it is not the only option. For effective estimation of quantities beside the energy, such as the LM matrix elements, other importance sampling functions are often preferred. [35, 46, 47] In our LM and blocked LM calculations in this study, we employ the importance sampling function (and the appropriately modified statistical estimate formulas [37])

$$|\Phi|^2 \equiv |\Psi|^2 + \frac{\epsilon}{M} \sum_I |D_I|^2 \qquad (3)$$

in which the D_I are the M different S_z-conserving single excitations relative to the closed shell reference determinant. The logic behind this choice is that it puts some weight on configurations that are highly relevant for the orbital rotation parameters' wave function derivatives, as small orbital rotations can be approximated via the addition of singles. We find that this importance sampling function substantially reduces the uncertainty of

the LM matrix elements corresponding to orbital rotations, which in turn helps reduce the update step uncertainty. For AD, we simply use traditional $|\Psi|^2$ importance sampling as in equation 2.

By the variational principle, we are guaranteed that E is an upper bound on the true ground state energy. Given some set of adjustable parameters in the functional form of Ψ, we expect that values of those parameters that yield a lower value of E to correspond to a wave function that is closer to the ground state. One could then imagine the abstract space produced by the possible values of all variational parameters. The set of optimal parameter values that specify the wave function expression which minimizes E can be taken as a point in this space labeled by the vector $\mathbf{p}^*$. In general, the initial choice for parameters will not be at this energy minimum point, but at some other point $\mathbf{p_0}$. The problem of determining the best wave function in VMC calculations then relies on an optimization algorithm for finding $\mathbf{p}^*$ after starting from $\mathbf{p_0}$.

Within this framework, one of the most important considerations is that the optimization is inherently stochastic due to the introduction of noise through the Monte Carlo evaluation of the integral in equation 2. This forms a contrast with many other methods in electronic structure theory including Hartree-Fock, CI, and coupled cluster where various deterministic optimization schemes predominate.[48] Many of the algorithms commonly encountered in a deterministic quantum chemistry context such as steepest descent and the Newton method, have been adapted for use in VMC.[49–53] However, there is now a need to be robust to the presence of noise. Historically, errors due to finite sampling led to numerical instabilities that prompted interest in minimizing variance[54, 55] instead of energy, but later optimization developments have sought to mitigate this issue and in this paper we only consider energy minimization. As we will now discuss in their respective sections, both the LM and gradient descent approaches possess features that enable them to operate stably in a stochastic setting.

The Linear Method

The LM[4, 56] begins with a first order Taylor expansion of the wave function. For a set of variational parameters given by vector $\mathbf{p}$, we have

$$\Psi(\mathbf{p}) = \Psi_0 + \sum_i \Delta p_i \Psi_i \tag{4}$$

where $\Psi_i = \frac{\partial \Psi(\mathbf{p})}{\partial p_i}$ and Ψ_0 is the wave function at the current parameter values.

Finding the optimal changes to the parameters amounts to solving the generalized eigenvalue problem

$$H\vec{c} = ES\vec{c} \tag{5}$$

in the basis of the wave function and its first order parameter derivatives $\{\Psi_0, \Psi_1, \Psi_2, ...\}$. H and S are the Hamiltonian and overlap matrices in this basis with elements

$$H_{ij} = \langle \Psi_i \,|\, H \,|\, \Psi_j \rangle \tag{6}$$

$$S_{ij} = \langle \Psi_i \,|\, \Psi_j \rangle \tag{7}$$

The matrix diagonalization to solve this eigenproblem for eigenvector $\vec{c} = (1, \Delta\mathbf{p})$ then yields the updated parameter values $\mathbf{p_1} = \mathbf{p_0} + \Delta\mathbf{p}$. As the matrices $\boldsymbol{H}$ and $\boldsymbol{S}$ both contain a subset of the second derivative terms that would be present in a Newton-Raphson approach, [57] the LM is most naturally categorized as a second-derivative method, and it certainly shares Newton-Raphson's difficulties with regards to dealing with matrices whose dimension grows as the number of variables.

For practical use with finite sampling, the LM must be stabilized to prevent unwisely large steps in parameter space. This is accomplished by adding shift values[4] to the matrix diagonal that effectively act as a trust radius scheme similar to those used with the Newton method. In our implementation, the Hamiltonian is modified with two shift values meant to address distinct potential problems in the optimization.[58]

$$\mathbf{H} \rightarrow \mathbf{H} + c_I\mathbf{A} + c_S\mathbf{B} \tag{8}$$

The matrix elements of $\mathbf{A}$ are given by $A_{ij} = \delta_{ij}(1 - \delta_{i0})$ so that the shift c_I effectively gives an energy penalty to directions of change from the current wave function.[4] The second shift is intended to address problems that may arise if some wave function derivatives have norms that differ by orders of magnitude. In this situation, the single shift value c_I is insufficient to preserve a quick yet stable optimization. For a parameter with a large derivative norm, a sufficiently high value of c_I might prevent an excessively large change in its value. However, all other parameter directions with smaller derivative norms will be so heavily penalized by the large value of c_I that those parameters become effectively fixed. The purpose of the second $c_S\mathbf{B}$ term is to retain important flexibility in other parameter directions. We can write the matrix $\mathbf{B}$ as

$$\mathbf{B} = (\mathbf{Q^T})^{-1}\mathbf{T}\mathbf{Q}^{-1} \tag{9}$$

where

$$Q_{ij} = \delta_{ij} - \delta_{i0}(1 - \delta_{j0})S_{0j} \tag{10}$$

and

$$T_{ij} = (1 - \delta_{i0}\delta_{j0})[\mathbf{Q^T}\mathbf{S}\mathbf{Q}]_{ij} \tag{11}$$

The matrix $\mathbf{Q}$ provides a transformation to a basis where all update directions are orthogonal to the current wave function and the matrix $\mathbf{T}$ is the overlap matrix in this

basis. The optimal choice of shift parameters c_I and c_S may depend on the particular optimization problem. In our implementation, an adaptive scheme adjusts the shifts on each iteration by comparing the energies calculated through correlated sampling on three different sets of shift values and choosing whichever shifts produced the lowest energy.

The LM has been successfully applied to a variety of systems to prepare good trial wave functions for DMC. [4, 28, 29, 57, 59–61] It has also been used in the variational optimization of a recent functional for targeting excited states.[31, 34, 37] However, it possesses a number of limitations, most notably a memory cost that scales with the square of the number of optimizable parameters due to the matrices it builds. This memory cost currently confines routine use of the LM to less than roughly 10,000 parameters though exceptional calculations with up to about 16,000 have been made.[11] Another shortcoming is the nonlinear bias of the LM. We are evaluating the elements of the Hamiltonian and overlap matrices stochastically and have a nonlinear relationship between them and our energy through the generally high order characteristic polynomial of the eigenvalue problem of equation 5. As a result, we in general expect the LM to converge to a point in parameter space slightly offset from the true minimum. This nonlinear bias has been studied for the LM in Hilbert space[62] and a similar issue arises in the context of Full Configuration Interaction QMC.[63] Both the memory constraint and the nonlinear bias of the LM become more severe for ansatzes with larger numbers of variational parameters, which spurs the search for potential alternatives. One approach suggested for memory reduction is to employ Krylov subspace methods for Eq. 4 to avoid building matrices, but it requires a drastically higher sampling effort due to the need for many matrix-vector multiplications and so we do not pursue the approach here.[5]

Blocked Linear Method

One recent approach to bypassing the memory bottleneck is known as the blocked linear method (BLM).[6] The first step of the algorithm is to divide the full set of parameters into N_b blocks. Next, a LM-style matrix diagonalization is carried out within each block and some number N_k of the resulting eigenvectors from the blocks are retained as good directions for constructing an approximation for the overall best update direction in the full parameter space. For a particular block of variables, the wave function expansion in the LM is given by

$$|\Psi_b\rangle = |\Psi_0\rangle + \sum_{i=1}^{M_b} c_i |\Psi^i\rangle \tag{12}$$

where $|\Psi^i\rangle$ is the wave function derivative with respect to the ith variable in the block, M_b is the number of variables in the block, and $|\Psi_0\rangle$ the current wave function as in the normal LM. We can perform the same matrix diagonalization done in the LM, only with parameters outside the block fixed. This yields a set of eigenvectors that we can use to construct another approximate expansion of the original wave function. We can construct a matrix $\mathbf{B}$ using the N_k eigenvectors with the lowest eigenvalues from each block and write a new expansion

$$|\tilde{\Psi}\rangle = \alpha |\Psi_0\rangle + \sum_{k=1}^{N_b} \sum_{j=1}^{N_k} A_{kj} \sum_{i=1}^{M_b} B_{ji}^{(b)} |\Psi^{i,b}\rangle \tag{13}$$

Having now pre-identified important directions within each block, the idea is that a subsequent LM-style diagonalization in the basis of these good directions (which yields the coefficients A_{kj}) should still provide a good update direction when re-expressed in the full parameter space.

In order to help retain most of the accuracy of the traditional LM, the first stage of the BLM computation includes N_o other good directions that are used to supply the current block's diagonalization with information about how its variables are likely to couple to those in other blocks. In practice, important out-of-block directions are obtained by keeping a history of previous iterations' updates as the optimization progresses. We can rewrite the one block expansion introduced in equation 12 as

$$|\Psi_b\rangle = |\Psi_0\rangle + \sum_{i=1}^{M_b} c_i |\Psi^i\rangle + \sum_{j=1}^{N_o} \sum_{k=1, k\neq b}^{N_b} d_{jk} |\Theta_{jk}\rangle \tag{14}$$

where we take the

$$|\Theta_{jk}\rangle = \sum_{l=1}^{M_k} C_{jkl} |\Psi^{l,k}\rangle \tag{15}$$

as the linear combinations of wave function derivatives from other blocks that were identified as important based on previous iterations' updates. The additional term in the expansion allows us to account for couplings between variables in different blocks and enable the construction of a better space for the second diagonalization. We assemble the matrix $\mathbf{B}$ and $|\tilde{\Psi}\rangle$ and then seek to minimize $\frac{\langle \tilde{\Psi} | H | \tilde{\Psi}\rangle}{\langle \tilde{\Psi} | \tilde{\Psi}\rangle}$ with respect to variational parameters α and A_{kj} in our BLM wave function expansion in equation 13.

Figure 1 portrays the algorithmic steps described above. Some number of parameters too large to be handled by the standard LM is divided among different blocks whose diagonalizations produce the vectors $\vec{b_i}$ for the construction of the space of the second diagonalization that produces the parameter update. The BLM can be thought of as achieving memory savings in the
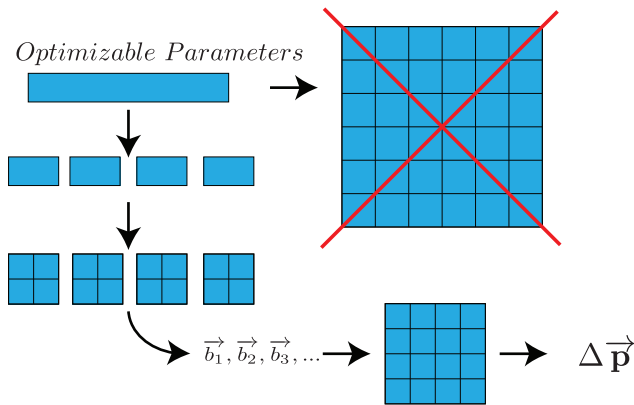
FIG. 1. Flowchart depicting steps in the BLM algorithm to arrive at a parameter update.

use of smaller matrices at the cost of having to run over the sample twice when the traditional LM must run over it just once. A more extensive description of the BLM and its precise memory usage can be found in its original paper.[6]

We divide parameters evenly among blocks, but one could implement the use of tailored blocks of varying sizes. It is advisable to choose the block size to be large enough to keep important parameters of the same type, such as all of those for a Jastrow factor, within the same block. This enables the expected strong coupling between them to be handled more accurately by the LM-style diagonalization within that block. While the BLM has been successfully applied up to about 25,000 parameters and found to closely reproduce the results of the standard LM, [6] it remains a relatively new method, and the present study will provide additional data on its efficacy.

Gradient Descent Methods

In the last few years, increasing attention[7–10, 64] has been paid to optimization methods that use only first derivatives to minimize a Lagrangian of the form

$$\mathcal{L}(\Psi(\mathbf{p})) = \langle \Psi \,|\, H \,|\, \Psi \rangle - \mu(\langle \Psi \,|\, \Psi \rangle - 1) \qquad (16)$$

where μ is a Lagrange multiplier and, in practice, a moving average of the local energy. There is no need to solve an eigenvalue problem as in the LM and the memory cost of these approaches scales linearly with the number of parameters. We also note that the stochastic evaluation of derivatives of this Lagrangian will lead to a smaller nonlinear bias compared to what is encountered in the LM. While there is some nonlinearity present in the product $\mu \langle \Psi \,|\, \Psi \rangle$, it is mild compared to the high order polynomials encountered in the solution of the LM eigenvalue problem and can be avoided entirely if desired through modest amounts of extra sampling. Minimization of this

Lagrangian targets the ground state, but excited states can similarly be targeted with these optimization algorithms merely by using derivatives of one of the excited state functionals that have been developed.[31, 65, 66]

The simplest method in this category is the steepest descent algorithm.

$$p_i^{k+1} = p_i^k - \eta_k \frac{\partial \mathcal{L}(\mathbf{p})}{\partial p_i} \qquad (17)$$

In this case, the value of each parameter on the $k+1$'th step is found simply by subtracting the statistically uncertain parameter derivative times a step size η_k. The step size can be taken as constant over all steps in the simplest case, but rigorous proofs on the convergence of stochastic gradient descent (SGD) rely on decaying step sizes satisfying $\sum_k \eta_k = \infty$ and $\sum_k \eta_k^2 < \infty$.[67]

It may be worth briefly commenting that the typical formulation of stochastic gradient descent as seen in the machine learning and mathematical optimization literature is slightly different from what we use here within VMC. In a common machine learning scenario,[67] one has a training set of input data $\{x_1, x_2, ..., x_n\}$ and corresponding outputs $\{y_1, y_2, ..., y_n\}$ and wishes to minimize a loss function $Q(x, y; w)$ that measures the error produced by a model $f_w(x)$, which predicts $\widetilde{y}_i$ given x_i and is parameterized by variables w. For this setting, the SGD algorithm refers to evaluating the gradient of Q with a randomly chosen pair (x_j, y_j) from the given data set and then computing the parameter update according to $w_{k+1} = w_k - \eta_k \nabla_w Q(x_j, y_j)$. For our VMC optimization, we are dealing with a noisy gradient similar to what occurs in this machine learning problem, but the source of our noise is somewhat different and lies in our means of evaluating the underlying 3N dimensional integrals within our Lagrangian derivatives. Another important distinction is that in machine learning applications, complete convergence to the minimum is in fact undesirable because it will overfit the model to the training data and degrade its performance on new sets of test inputs. Much as SGD provides a computational speed up for machine learning problems, we are also able to operate gradient descent methods at a cheap per-iteration cost because we need only a modest number of samples to evaluate sufficiently precise Lagrangian derivatives compared to the Hamiltonian and overlap matrices in the LM. However, unlike the machine learning case, we do want to come as close as possible to the true minimum, and we will see that even reaching the vicinity of the minimum can be difficult for descent methods when typical VMC initial guesses are employed.

While steepest descent can be guaranteed to eventually reach the minimum of the Lagrangian even in a stochastic setting, its asymptotic convergence is very slow. For some intuition, one could imagine the landscape of the Lagrangian's values forming a very narrow valley near the true minimum. In this situation, steepest descent

$$q_i^{k+1} = p_i^k - \tau_k \frac{\partial \mathcal{L}(\mathbf{p})}{\partial p_i} \qquad (19)$$

$$\lambda_0 = 0 \qquad \lambda_k = \frac{1}{2} + \frac{1}{2}\sqrt{1 + 4\lambda_{k-1}^2} \qquad \gamma_k = \frac{1 - \lambda_k}{\lambda_{k+1}} \qquad (20)$$

$$\tau_k = \frac{\eta}{\sqrt{E[(\frac{\partial \mathcal{L}}{\partial p_i})^2]^{(k)}} + \epsilon} \qquad (21)$$

$$E[(\partial \mathcal{L})^2]^{(k)} = \rho E\left[\left(\frac{\partial \mathcal{L}}{\partial p_i}\right)^2\right]^{(k-1)} + (1-\rho)\left(\frac{\partial \mathcal{L}}{\partial p_i}\right)^2 \quad (22)$$

Above, p_i^k denotes the value of the ith parameter on the kth step of the optimization, τ_k is a step size that is adaptively adjusted according to the RMSprop algorithm in equations 21 and 22. The running average of the square of parameter derivatives in the denominator of τ_k allows for the step size to decrease when the derivative is large, which should hedge against the possibility of taking excessively large steps. Conversely, a smaller denominator when the derivative is small allows for larger steps to be taken. The weighting in the running average is controlled by a factor ρ that can be thought of as the amount of memory retained of past gradients for adjusting τ_k, and η again denotes the chosen initial step size. In order to avoid possible singularities when the gradient is very close to zero, a small positive number ϵ is included in the denominator of τ_k. Equation 18 shows the momentum effect in which the update for the parameter on the $k+1$ step depends on the update from the previous step as well as the current gradient. We also follow the Booth group in applying a damping factor to the momentum by replacing γ_k with $\gamma_k e^{-(\frac{1}{d})(k-1)}$. The quantity d effectively controls how quickly the momentum is turned off, which eventually turns the algorithm into SGD. The values of d, η, ρ, and ϵ may all be chosen by the user of the algorithm and are known as hyperparameters in the machine learning literature. In the results we present using this method, we have used $d = 100$, $\rho = .9$ and $\epsilon = 10^{-8}$. We have found adjusting these hyperparameters has relatively little influence on optimization performance compared to choices for step size η, but their influence could be explored more systematically.

The Clark group's algorithm takes a far simpler form

$$p_i^{k+1} = p_i^k - \alpha\eta \frac{\left|\frac{\partial \mathcal{L}}{\partial p_i^k}\right|}{\frac{\partial \mathcal{L}}{\partial p_i^k}} \qquad (23)$$

and has been recently used with neural network wave functions in the context of the Hubbard model.[10] Here α is a random number in the interval $(0, 1)$ and η sets the overall scale of the random step size. The motivation for allowing the step size to be random is that it may help
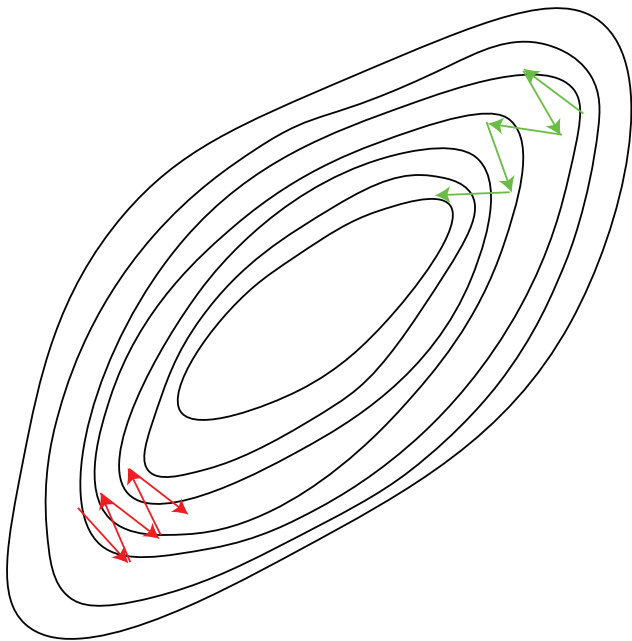

FIG. 2. Illustration of the difficulty faced by steepest descent in red on the lower left with its slow approach to the minimum. Accelerated descent in green on the upper right is able to progress more rapidly to the minimum with its memory of previous gradients.

would produce parameter updates mostly back and forth along the sides of the valley with little improvement of parameter values in the direction directly toward the minimum. Due to the limitations of steepest descent, a number of other flavors of accelerated gradient descent (AD) have been developed that include a momentum term with information on previous values of the gradient. As illustrated in Figure 2, the general intuition is that this additional term provides some memory of the progression along narrow valleys that steepest descent lacks and thereby achieves swifter convergence. In addition, there are multiple schemes for adaptively varying the step sizes used in a manner that draws on the particular derivative values for each individual parameter as the optimization progresses. These methods have recently been applied successfully to Hilbert space QMC. In this study, we work in real space and investigate a combination of Nesterov momentum with RMSprop as presented by the Booth group [7, 64], a method using random step sizes from the Clark group[10], AMSGrad, recently used by the Sharma group[8, 9], as well as the ADAM optimizer[68].

We now lay out the precise expressions for each of these methods in turn. The RMSprop algorithm used by Booth and co-workers is given by the following recurrence relations.[7]

$$p_i^{k+1} = (1 - \gamma_k)q_i^{k+1} - \gamma_k q_i^k \qquad (18)$$

the optimization escape local minima that it encounters. Within VMC, this algorithm can be run with fewer samples per iteration even compared to other gradient descent based algorithms as only the sign of the derivative needs to be known, but it typically requires many more iterations to converge.

ADAM and AMSGrad are popular methods within the machine learning community[68–70] and have similar forms. ADAM is given by:

$$p_i^{k+1} = p_i^k - \eta \frac{m_i^k}{\sqrt{n_i^k}} \tag{24}$$

$$m_i^k = (1 - \beta_1)m_i^{k-1} + \beta_1 \frac{\partial \mathcal{L}}{\partial p_i^k} \tag{25}$$

$$n_i^k = \beta_2 \, n_i^{k-1} + (1 - \beta_2)\left(\frac{\partial \mathcal{L}}{\partial p_i^k}\right)^2 \tag{26}$$

AMSGrad is a recent adaptive step size scheme developed in response to the limitations of ADAM [70] and has almost the same form except for a slightly different denominator.

$$n_i^k = \max\left(n_i^{k-1}, \ (1 - \beta_2)\, n_i^{k-1} + \beta_2\left(\frac{\partial \mathcal{L}}{\partial p_i^k}\right)^2\right) \tag{27}$$

In our calculations, we have used $\beta_1 = 0.1$ and $\beta_2 = 0.01$ for both AMSGrad and ADAM in line with the choice made by the Sharma group.[8, 9] It may be worth noting that a different convention appears in machine learning literature using $1 - \beta_1$ and $1 - \beta_2$ for what we and the Sharma group call β_1 and β_2. [69, 70]

Compared to the LM, these first derivative descent methods have some significant advantages. Their low memory usage and reduced nonlinear bias make them a natural fit for the large parameter sets that the LM struggles to handle. They are remarkably robust in the presence of noise and do not need special safeguards against statistical instabilities such as the LM's shifts. At a basic practical level, the descent methods are also far simpler to implement than the LM and especially its blocked variant. However, as we will see in our results, they often struggle to reach the vicinity of the minimum using a comparable sampling effort.

A Hybrid Optimization Method

In an attempt to retain the benefits of both the LM and the AD techniques, we have developed a hybrid optimization scheme that can be applied to large numbers of parameters. Our approach alternates between periods of optimization using AD and sections using the BLM. Among other advantages, this allows us to use gradient
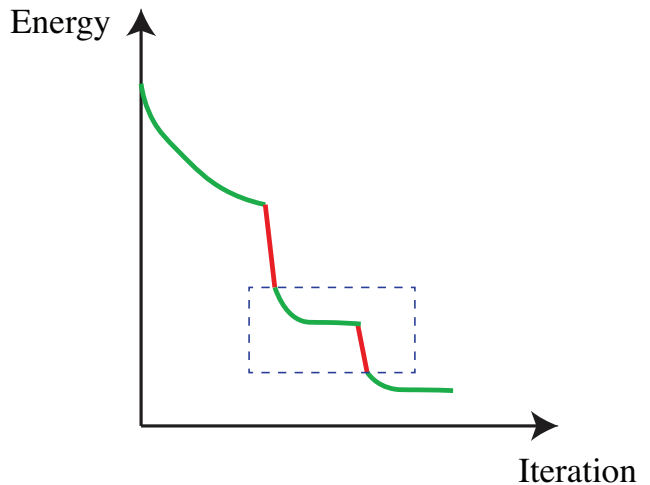

FIG. 3. Schematic depiction of a typical energy optimization using the hybrid method. The dashed box around a section of descent in green and BLM in red defines a macro-iteration of the method.
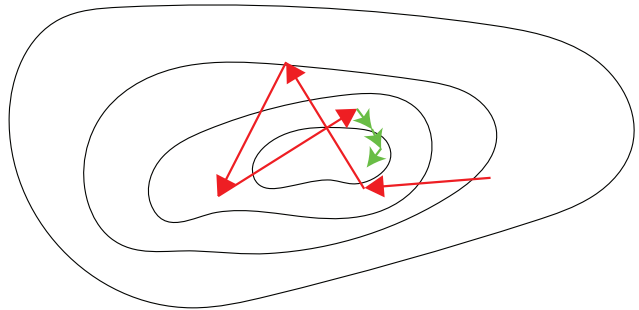

FIG. 4. Schematic representation of gradient descent corrections in green to the red BLM steps, which we have observed to produce a greater degree of uncertainty about the location of the final minimum.

descent to identify the N_o previous important directions in parameter space that are used in the BLM via equation 14. The precise mixture of both methods can be flexibly altered, but a concrete example would be to first optimize for 100 iterations using RMSprop. By storing a vector of parameter value differences every 20 iterations, we would produce 5 vectors that can be used for equation 14 in some number (say three) steps of the BLM. After the execution of these BLM steps, the algorithm would return to another 100 iterations of descent and the process repeats until the minimum is reached. Figure 3 shows a generic depiction of how the ground state energy optimization may behave over the course of the hybrid method. There are extended sections of computationally cheap optimization using gradient descent interwoven with substantial energy improvement over a few BLM steps.

The use of AD and the BLM should naturally allow parameter sets beyond the traditional LM limit of about

10,000 variables to be addressed, a limit we will surpass in the present study in the diflurodiazene system. For now, Table I lays out how the memory cost of the methods we are considering scales with number of parameters N. Both the hybrid method and the BLM steps it contains have a memory scaling that is intermediate between that of the standard LM and the descent methods. The cost is given only approximately because while it is normally dominated by the cost of the N_b blocks in the BLM, there are additional contributions related to how many directions are retained from the first BLM diagonalization and how many old directions are used.[6]

TABLE I. Rough memory cost scaling for the optimization methods we examine, with N the number of optimized parameters and N_b the number of blocks

Method Type	Memory Cost
Standard Linear Method	$O(N^2)$
Blocked Linear Method	$\sim O\left(\frac{N^2}{N_b}\right)$
Hybrid Method	$\sim O\left(\frac{N^2}{N_b}\right)$
Descent Methods	$O(N)$

One key motivation for including sections of AD, especially when the method is near convergence, is to counteract the noise we observe in LM updates. While the LM tends to converge in a relatively small number of steps, we find the individual energies still fluctuate from iteration to iteration by multiple mE_h, particularly when we are working with wave functions that possess many highly nonlinear parameters. Figure 4 shows a cartoon of this behavior near the minimum that prevents tight convergence. Unless the shifts are large enough to constrain it to very small steps, the LM will tend to bounce around near the true minimum due to substantial (and biased) statistical uncertainties in its step direction. The resulting energy fluctuations lead to ambiguity in what to report as the definitive LM energy. One could take the absolute lowest energy reached on any iteration, but this is fairly unsatisfactory as it feels too dependent on a "lucky" step landing right on the minimum. Our practice has been to take an average over multiple steps at the end of the optimization when parameter values should be converged. However, this will generally include iterations with upward energy deviations due to the step uncertainties. The use of AD offers a way out of this dilemma because it can correct the errors in the LM steps by moving towards the minimum more smoothly and with less bias. As we shall demonstrate in our results, these considerations seem to give the hybrid method a statistical advantage over the LM by achieving lower error bars for the same computational cost. They are also the basis of our recommendation for finishing optimizations with

a long section of pure AD, which we shall show tends to improve the energy and greatly diminish the final statistical uncertainty.

Wave Functions

An assessment of optimization methods' effectiveness requires consideration of the form of the wave function that they are applied to. Multi-Slater determinant wave functions have been a common choice of ansatz in QMC and are typically combined with Jastrow factors that help recover some electron correlation and describe particle cusps.[41] We specify our Multi-Slater Jastrow (MSJ) wave function with the following set of equations.

$$\Psi = \psi_{MS}\psi_J\psi_C \qquad (28)$$

$$\psi_{MS} = \sum_{i=0}^{N_D} c_i D_i \qquad (29)$$

$$\psi_J = \exp\sum_i\sum_j \chi_k(|r_i - R_j|) + \sum_k\sum_{l>k} u_{kl}(|r_k - r_l|) \qquad (30)$$

$$\psi_C = \exp(\sum_{IJ} F_{IJ} N_I N_J + \sum_K G_K N_K) \qquad (31)$$

In equation 29 above, ψ_{MS} consists of N_D Slater determinants D_i with coefficients c_i. It can be generated by some other quantum chemistry calculation such as complete active space self-consistent field (CASSCF) or a selective CI method prior to the VMC optimization. In the one- and two-body Jastrow factor ψ_J, we have functions χ_k and u_{kl}, which are constructed from optimizable splines whose form is constrained so as to enforce any relevant electron-electron and electron-nuclear cusp conditions. [58]

While MSJ wave functions with these types of traditional Jastrow factors (TJFs) have been successfully used in many contexts, [4, 11, 14, 37, 41] more involved correlation factors can be considered. Typically, this involves the construction of many-body Jastrows factors, [55, 71, 72] which may involve various polynomials of interparticle distances [26, 27, 71] or an expansion in an atomic orbital basis [24, 72–77] or a set of local counting functions. [28, 29] The latter case of many-body Jastrows, known as real space number-counting Jastrow factors (NCJF), is employed here as an example many-body Jastrow factor. In real space, Jastrow factors have historically been effective at encoding small changes to the wave function associated with weak correlation effects, [41] but work in Hilbert space and lattice model

VMC reminds us that they can also be used to aid in the recovery of strong correlations. [40, 78, 79] One way to view NCJFs is as an attempt to develop a real space many-body Jastrow factor that can aid in recovering both strong and weak electron correlations. [29]

The form of our NCJFs in equation 31 has the same structure as previously proposed four-body Jastrow factors,[75] where N_I denotes the population of a region and the F_{IJ} and G_K are linear coefficients. The region populations are computed by summing the values of counting functions at each electron coordinate.

$$N_I = \sum_i C_I(\mathbf{r_i}) \tag{32}$$

In this work, we use a recently introduced [29] form for the counting functions consisting of normalized Gaussians.

$$C_I = \frac{g_I(\mathbf{r})}{\sum_j g_j(\mathbf{r})} \tag{33}$$

where

$$g_j(\mathbf{r}) = \exp((\mathbf{r} - \mu)^T \mathbf{A}(\mathbf{r} - \mu) + K) \tag{34}$$

describes a Gaussian about a center μ. By placing these normalized Gaussians at various centers, we can divide up space with a Voronoi tessellation. Schemes have been developed to generate partitions that either consist of regions centered on atoms or of finer grained divisions of space that can capture correlation within an atomic shell. We make use of both types of partitioning methods for different wave functions in our study. For simplicity, we only consider optimization of the parameters F_{IJ} in the F-matrix of our NCJFs (the coefficients G_K can be eliminated with a basis transformation of the region populations N_I), [29] but in principle the parameters defining the Gaussians g_j could also be optimized. We provide details of the Gaussians used in our ansatzes in Appendix D.

We also consider the problem of optimizing the molecular orbital shapes alongside the other variational parameters. The ability to relax orbitals is important for successful study of many systems, particularly those involving excited state phenomena.[37] We make use of considerable theoretical and computational machinery based on the table method enhancements developed by Filippi and coworkers [13, 14] that enables efficient evaluation of orbital rotation derivatives in large MSJ wave functions. A rotation of molecular orbitals can be described with a unitary transformation with matrix $\mathbf{U}$ parameterized as the exponential of an antisymmetric matrix $\mathbf{X} = -\mathbf{X^T}$

$$\mathbf{U} = \exp(\mathbf{X}) \tag{35}$$

Impressively, one can obtain all wave function derivatives with respect to the elements of $\mathbf{X}$ for a large multi-Slater

determinant ansatz for a cost that is only slightly higher than that of the local energy evaluation. For the details of how this is accomplished, we refer the reader to the original publications. [13, 14] From the standpoint of parameter optimization, the main significance of the orbitals (and the NCJFs) lies in both their nonlinearity and their strong coupling to other optimizable parameters. In practice, we find that turning on the optimization of orbitals and NCJFs greatly enhances the difficulty of the optimization problem compared to MSJ optimizations in which only the CI coefficients and one- and two-body Jastrow parameters are varied.

RESULTS

Multi-Slater Jastrow N$_2$

For a small initial test system, we consider the nitrogen dimer N$_2$ at the near-equilibrium and stretched bond lengths of 1.1 and 1.8 Å. The nitrogen dimer is a known example of a strongly correlated system and a common testing ground for quantum chemistry methods.[40, 79–84] The initial wave function ansatz consists of a modest number of Slater determinants (67 for the equilibrium geometry and 169 for the stretched, the result of a 0.01 cutoff limit on determinant coefficients) with traditional one-body and two-body Jastrow factors. The Jastrow splines provide 30 additional optimizable parameters via 10 point cubic b-splines with cutoff distances of 10 bohr for the electron-nuclear and same-spin and opposite-spin electron-electron components. The Slater determinant expansion is the result of a (10e,12o) CASSCF calculation in GAMESS[85] using BFD pseudopotentials and the corresponding VTZ basis set.[86] Due to the simplicity of the variable space in this case, we have employed the $|\Psi|^2$ guiding function for all optimization methods, including the LM and BLM. See Appendix B for further computational details.

The first and simplest study we can make is to optimize our ansatzes with our multiple optimization techniques until convergence and compare final energies. Note that all of our VMC optimizations with different methods in this study were performed using our implementations within a development version of the QMCPACK software package.[58] As N$_2$ is a small enough system that the traditional LM can be easily employed, we take the approach of first obtaining a traditional LM optimization result and then using it as a reference against which to compare the performance of other methods. For the gradient descent methods, multiple optimizations were attempted with the initial step sizes tweaked from run to run based on a rough examination of how parameter values compared to the LM's results. We find that the chosen values for the step sizes and other hyperparameters in the gradient descent algorithms often leads to
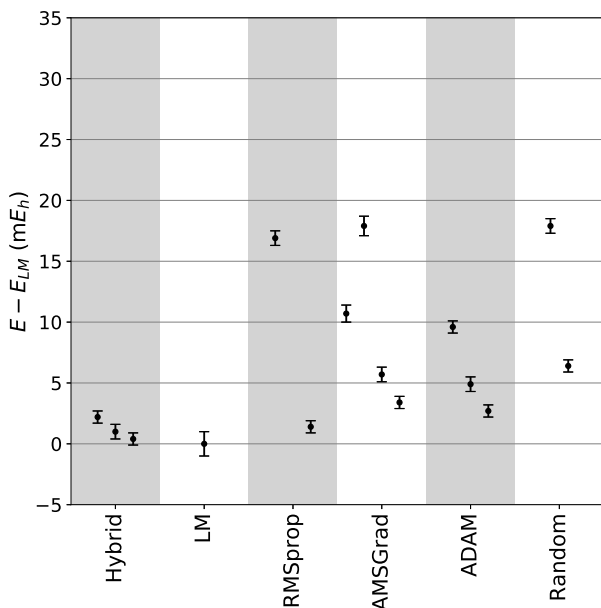
FIG. 5. Different methods' optimized energies relative to that of the LM for equilibrium N_2 when optimizing CI coefficients and the TJF.

FIG. 6. Different methods' optimized energies relative to that of the LM for stretched N_2 when optimizing CI coefficients and the TJF.

apparent convergence at different energies. It is therefore essential to make effective choices for these parameters, which in part seems to rely on one's experience with a given system.

Figures 5 and 6 show energy differences relative to the LM result when optimizing the equilibrium and stretched nitrogen dimer wave functions respectively. Tables providing the precise energies and statistical uncertainties as well as the step sizes used are shown in the appendices. First, we see the choice of step sizes can have a substantial influence on the quality of gradient descent results. In some cases, the same method can appear to converge to energies more than 20 mE_h apart when run with different initial step sizes. While many of the gradient descent optimizations clearly did not reach the minimum, the energy differences from the LM are only about 5 mE_h or less when looking at the runs that used what turned out to be the best choices for the hyperparameters. With further tweaking of the hyperparameters, we would guess that at least some of these descent methods could match the performance of the LM in this simple test case. Finally, we observe that the hybrid method performs about as well as the best descent optimizations, typically reaching energies that agree with the LM within error bars.

All parameter N_2

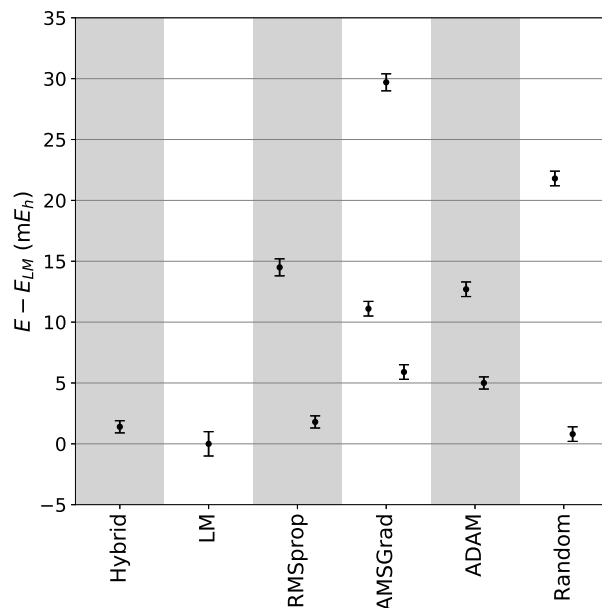We now add a NCJF and enable orbital optimization in order to extend the comparison in a setting with a larger number and variety of nonlinear parameters. We will consider the relative merits of the optimization methods in much greater detail in this setting as it offers a clearer view of their differences. For the number-counting Jastrow factor, we generated a set of 16 counting regions with 8 octants per atom after dividing space in half with a plane bisecting the bond axis. The details are given in Appendix D, but we will note here that this adds 135 F-matrix parameters to the optimization. Allowing for orbital optimization adds another 663 and 618 parameters for the equilibrium and stretched cases, respectively. Note that our implementation of orbital optimization in QMCPACK removes rotation parameters for orbitals that are not occupied in any determinant and also between orbitals occupied in all determinants, and so the precise number of rotation parameters is a function of the determinant expansion. With orbital optimization enabled, the choice of importance sampling function becomes an issue, and we now employ $|\Phi|^2$ for all LM and BLM steps with the ϵ weight set to 0.001.

Figures 7 and 8 show converged ground state energies relative to that of the LM. For this more difficult version of the nitrogen dimer, we find that the gradient descent methods are less effective. They now often yield energies that can be 10 mE_h or more above the LM's answer though we again find that choice of step size plays a significant role. The worst results for AMSGrad and ADAM were the result of choosing inappropriately large step sizes and simple reductions in the initial step size produced improvements in energy of tens of mE_h though the final result still remained well above the LM's. When we examined the optimizations over the course of
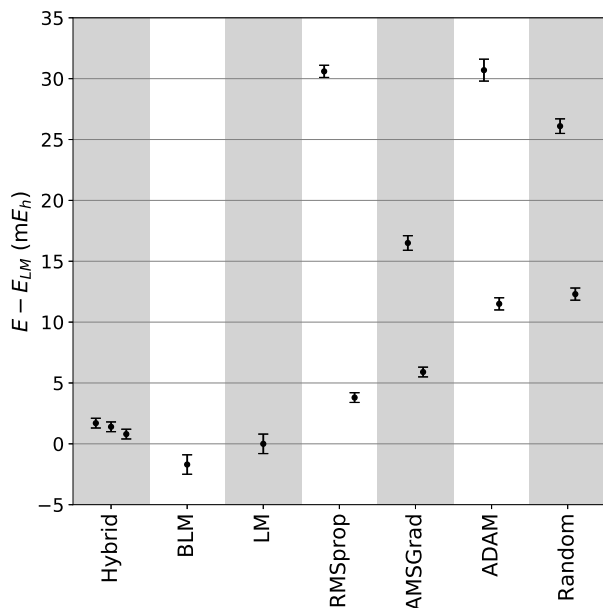
FIG. 7. Different methods' optimized energies relative to that of the traditional LM for equilibrium N_2 when all parameters are optimized simultaneously. See also Table II.

FIG. 8. Different methods' optimized energies relative to that of the traditional LM for stretched N_2 when all parameters are optimized simultaneously. See also Table III.

their iterations, the gradient methods typically displayed some ability to quickly improve the wave function and energy initially, but they would then plateau and only very slowly improve the energy thereafter. Extrapolating from our results indicates that even if these gradient descent methods eventually converge to the minimum, they will only do so after thousands more iterations and at a computational cost well beyond that of the LM.

A more careful comparison of the different methods can be made by referring to Tables II and III, which list the precise converged energies and their error bars. We also report the total number of samples used in each optimization as a proxy for computational effort, noting that for the BLM and the BLM portion of the hybrid method we double counted samples out of fairness as the BLM steps require running over their samples twice. In assessing cost, one must also consider the statistical uncertainty achieved, where we see that the LM and BLM are at a disadvantage. To help illustrate the update uncertainty contribution to this error, which we first discussed in the theoretical section above, we show the energy versus LM iteration for equilibrium N_2 in Figure 9. The fluctuations in energy from step to step, sometimes by as much as 2 mE_h, demonstrate the difficulty the LM faces from the uncertainty in its steps near the minimum. In this case, we see that the LM's final energy uncertainty is driven by the update step uncertainty rather than the uncertainty in evaluating the energy for a given set of parameter values at a particular iteration. We have observed similar behavior in the BLM and include the result of a BLM calculation in the tables. Note that the tabulated ener-
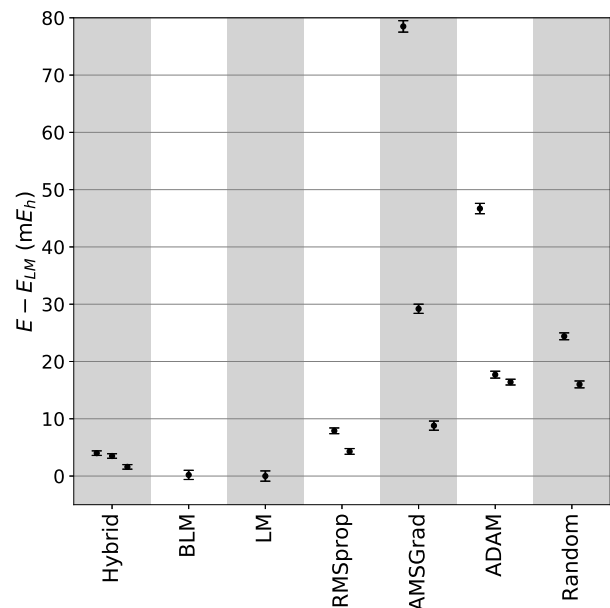
TABLE II. Energies, uncertainties, and sample numbers for optimization of all parameters in equilibrium N_2.

Method	Energy (a.u.)	Uncertainty (a.u.)	Samples
Hybrid 1	-19.9263	0.0004	5,400,000
Hybrid 2	-19.9266	0.0004	10,000,000
Hybrid 3	-19.9272	0.0004	42,000,000
RMSprop 1	-19.8974	0.0005	20,000,000
RMSprop 2	-19.9242	0.0004	20,000,000
AMSGrad 1	-19.9115	0.0006	20,000,000
AMSGrad 2	-19.9221	0.0004	20,000,000
ADAM 1	-19.8973	0.0009	20,000,000
ADAM 2	-19.9165	0.0005	20,000,000
Random 1	-19.9019	0.0006	20,000,000
Random 2	-19.9157	0.0005	20,000,000
LM	-19.9280	0.0008	40,000,000
BLM	-19.9297	0.0008	80,000,000
DF-BLM	-19.9293	0.0001	90,000,000
DF-Hybrid 1	-19.9290	0.0001	15,400,000
DF-Hybrid 2	-19.9290	0.0001	20,000,000
DF-Hybrid 3	-19.9293	0.0001	52,000,000

gies come from an average over the last ten optimization steps in the case of the standard LM and BLM and from an average over the last 50 descent steps in the case of the hybrid and pure descent methods.

From the tabulated data, we see that the hybrid optimization can achieve lower energies than the gradient descent methods using fewer samples, and that its re-

TABLE III. Energies, uncertainties, and sample numbers for optimization of all parameters in stretched N_2.

Method	Energy (a.u.)	Uncertainty (a.u.)	Samples
Hybrid 1	-19.6316	0.0004	5,400,000
Hybrid 2	-19.6321	0.0004	8,400,000
Hybrid 3	-19.6340	0.0004	49,200,000
RMSprop 1	-19.6277	0.0005	20,000,000
RMSprop 2	-19.6313	0.0005	20,000,000
AMSGrad 1	-19.5571	0.0010	20,000,000
AMSGrad 2	-19.6064	0.0008	20,000,000
AMSGrad 3	-19.6268	0.0008	20,000,000
ADAM 1	-19.5889	0.0009	20,000,000
ADAM 2	-19.6179	0.0006	20,000,000
ADAM 3	-19.6192	0.0005	20,000,000
Random 1	-19.6112	0.0006	20,000,000
Random 2	-19.6196	0.0006	20,000,000
LM	-19.6356	0.0009	40,000,000
BLM	-19.6354	0.0008	80,000,000
DF-BLM	-19.6356	0.0001	90,000,000
DF-Hybrid 1	-19.6352	0.0001	15,400,000
DF-Hybrid 2	-19.6354	0.0001	18,400,000
DF-Hybrid 3	-19.6346	0.0001	59,200,000

FIG. 9. The standard LM optimization for all parameter equilibrium N_2.

FIG. 10. Values for the first off-diagonal F-matrix element (F_{01}), the first electron-nuclear TJF spline parameter (u_0), and the second orbital rotation variable (X_{02}) at each micro iteration of the "Hybrid 1" optimization for all parameter equilibrium N_2.
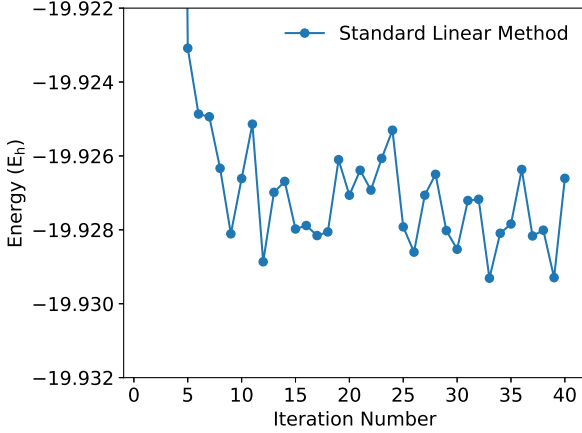
sults are typically within a few mE_h of the traditional LM. While the accelerated descent sections of the hybrid method provide some swift energy reductions early on when the wave function is still far from the minimum in parameter space, the BLM steps in the algorithm greatly accelerate the process of bringing the parameters near to the minimum, as can be seen in Figure 10. Looking at the electron-nuclear spline parameter and the orbital rotation parameter, we see typical cases in which rapid initial parameter movement during the early part of the first RMSprop stage transitions to much slower move-
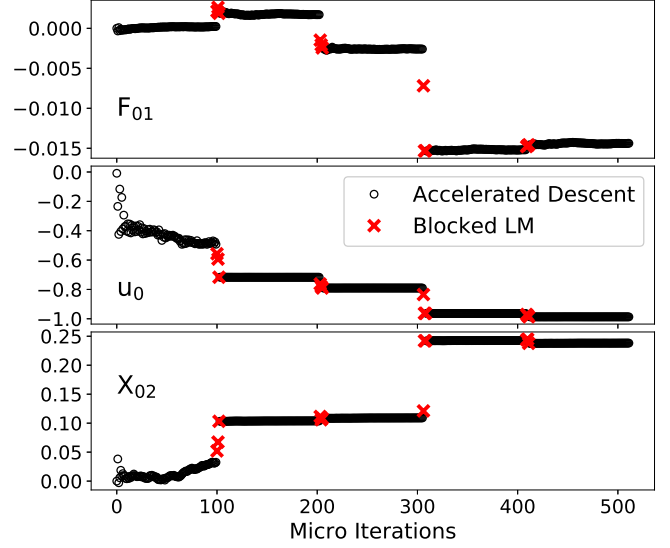
ment later in that stage, followed by very little movement at all in later RMSprop stages. Note that the latter can be explained largely by the need to keep initial step sizes small in later stages to avoid significant upward deviations in the energy as the RMSprop method rebuilds its momentum history. In between these AD stages, the BLM updates move the parameter values in much larger steps, greatly accelerating convergence. This behavior makes the hybrid approach somewhat more black box as compared to the pure descent approaches, as the ability to get near the minimum with a modest sampling effort is much less dependent on the choice of the initial step sizes than for the AD methods. This conclusion is supported by the fact that the hybrid optimizations in Tables II and III used various initial step size settings (as discussed in Appendix B) and nonetheless produced lower energies than the pure descent methods in every case.

As discussed in our introduction of the hybrid method, another advantage is its ability to obtain a lower error bar at convergence than the LM for the same overall computational cost. This is a natural consequence of spending part of its sampling effort on gradient descent steps that correct for the BLM steps' uncertainty and bias (as illustrated earlier in Figure 4) and that hew closer to the zero-variance principle by importance sampling with $|\Psi|^2$. To demonstrate this advantage explicitly, we ran additional sets of LM and hybrid optimizations adjusted to have essentially the same total number of samples. We then compare the standard error for the last ten LM steps and the last ten hybrid macro iterations in Figures 11 and 12, where we find that the hybrid has a substantially lower
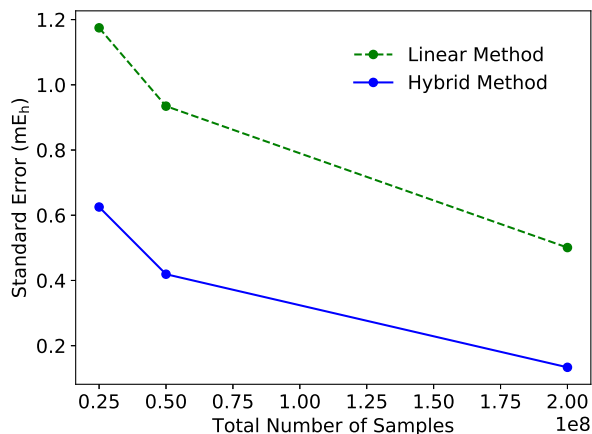
FIG. 11. Standard Errors for the hybrid method and LM on all parameter equilibrium N_2 vs different optimizations' total sampling costs.
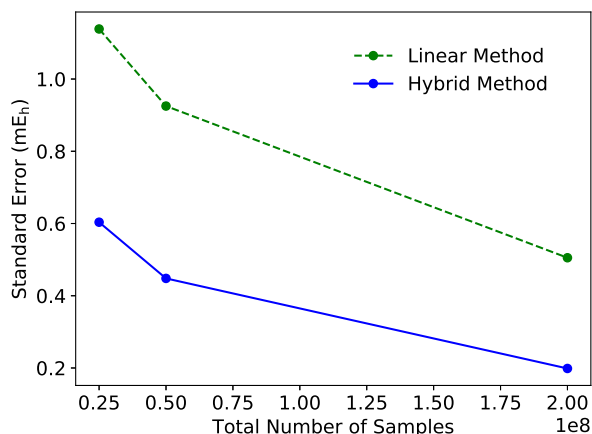

FIG. 12. Standard Errors for the hybrid method and LM on all parameter stretched N_2 plotted against different optimizations' total sampling costs.

FIG. 13. Converged energies in equilibrium N_2 before and after a final descent optimization.
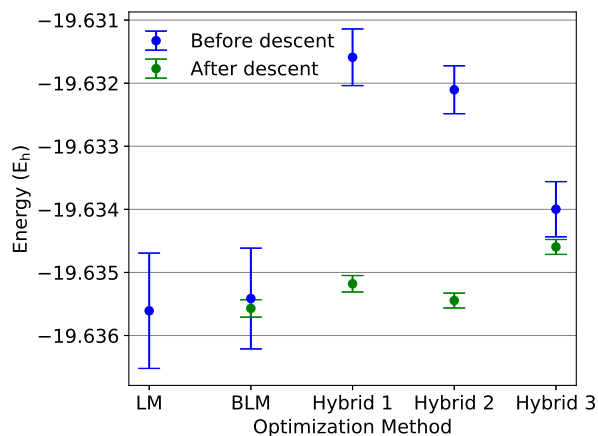
FIG. 14. Converged energies in stretched N_2 before and after a final descent optimization.

statistical uncertainty in every case. Assuming the usual $N^{-1/2}$ decay of uncertainty with sample size, the LM would require a factor of roughly four times more samples to reach the hybrid's uncertainty,

These statistical advantages in the final energy can be improved even further if we finish an optimization with a long section of pure descent. To demonstrate this, we have taken the final wave functions produced by the hybrid and BLM optimizations in Tables II and III and applied a further period of optimization using RMSprop with initial step sizes of 0.001 for all parameters. This "descent finishing" (DF) adds only a modest additional cost compared to the preceding optimization and yields a large improvement in statistical uncertainty and, in many cases, an improvement in the final energy value as well. These advantages can be seen clearly in Figures 13 and

14, as well as in Tables II and III, where we observe final error bars that are a factor of eight smaller than those of the LM. In terms of cost, this implies that the traditional LM would have required 64 times the original number of samples to achieve the DF-BLM or DF-hybrid precision. Put another way, we find that the DF-hybrid approach gives an equivalent or lower energy, with a much smaller error bar, at a substantially lower cost. Note that, in contrast, we find that this DF approach is not very effective when used in conjunction with the pure descent methods, where it essentially amounts to restarting the methods at the parameter values found after the first run of their optimization. While we do find that this restarting of the accumulation of momentum can improve the energy, the wave function parameters still do not reach their optimal values and the energy lowering vs total sampling cost is not competitive with the DF-hybrid.

Our study of the nitrogen dimer provides some clarity

FIG. 16. Converged energies in equilibrium styrene before and after a final descent optimization.

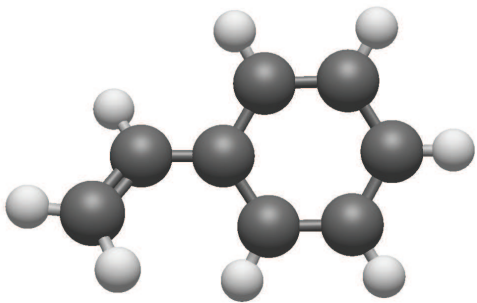FIG. 15. Equilibrium geometry of styrene. See Appendix C for structure coordinates.

on the relative strengths of the LM and gradient descent, while also pointing the way to a more effective synthesis of the two. Gradient descent methods struggle in the presence of a variety of different highly nonlinear parameters, although they did perform better when we were only optimizing TJFs and CI coefficients. Among the descent methods, we found that the RMSprop approach came the closest to achieving the LM minimum energy. It is of course difficult to rule out the possibility that this and other AD methods could reach the LM energy with additional sampling and more experimentation with the hyperparameters. However, it is far from obvious that this would be be cost-competitive, and the need to make careful and possibly system-specific choices for hyperparameters is somewhat antithetical to the general aspiration that an optimizer be as black-box as possible. For its part, the LM is more effective at moving parameters into the vicinity of the minimum, but tight convergence is then stymied by an unsatisfactory level of biased statistical uncertainty. As a side note, this behavior — in which the first derivative methods give better convergence once near the minimum but are at a relative disadvantage far from the minimum — is somewhat the reverse of what one would expect in deterministic optimization, where second derivative methods are at their strongest relative to first derivative methods during the final tight convergence in the vicinity of the minimum. Although things are reversed in the stochastic VMC case, we stress that the two classes of methodology are strongly complementary, as they compensate for each other's weaknesses. By using a low-memory version (BLM or hybrid) of the LM to get near to the minimum and then handing off to an accelerated descent method to achieve tight convergence, we find better overall performance than when working
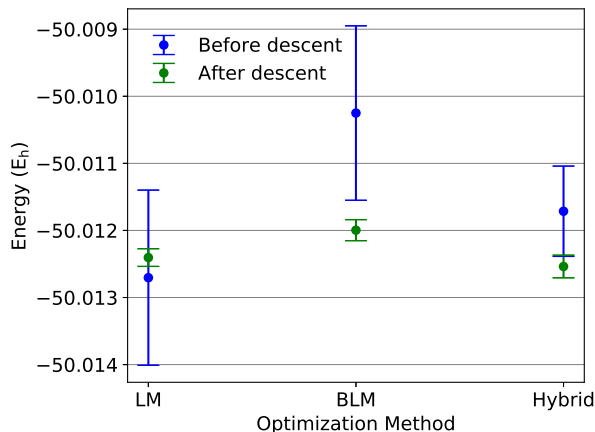
with either class of method on its own. These insights in hand, we will now apply this combined approach in a pair of larger and more challenging VMC optimization examples.

Styrene

We first turn to styrene at its equilibrium geometry (Figure 15) which offers an optimization with both more electrons and more variables, but in which the traditional LM is still quite achievable for comparison. As in N_2, we construct a multi-Slater wave function modified by both TJFs and a NCJF. To generate our Slater determinants, we have employed the heatbath selective CI (HCI) method as implemented in the Dice code by Sharma and coworkers. [16, 18] The orbital basis for the HCI calculation was produced via a (14e,14o) CASSCF calculation in Molpro [87] using a recently developed set of pseudopotentials and their corresponding double zeta basis.[88] In this CASSCF basis, HCI then correlated 32 electrons (out of a total of 40 electrons left over after applying pseudopotentials) in 64 orbitals. For our NCJF, we defined one counting region per atom, giving our F-matrix 135 optimizable parameters (see Appendix D for further NCJF details).

We optimized our wave function in a staged fashion using the standard LM, the BLM, and the hybrid method. First, we conducted a partial optimization of the TJFs and the 100 most important CI coefficients. We then turned on the optimization of the orbitals and the NCJF's F-matrix, reaching a total of 4,570 parameters, most of them highly nonlinear. In the hybrid and BLM optimizations, the parameters were divided into 5 blocks and we used $N_k = 50$ and $N_o = 5$ for our numbers of kept directions and previous important directions, re-

TABLE IV. A summary of the VMC optimization stages in FNNF showing the number of determinants N_d included from HCI, which parameters are optimized, and the total number N_p of optimized parameters. Note that CI coefficients are optimized at every stage. Stages 2, 3, and 4 start from the parameter values from the previous stage, with newly added determinants' coefficients initialized to zero. We also report the number of iterations performed in each stage, which for stage 4 is simply the number of RMSprop steps. A hybrid iteration, on the other hand, consists of 100 RMSprop steps followed by three BLM steps. All RMSprop steps use 20,000 samples drawn from $|\Psi|^2$, while the BLM steps each use 1 million samples drawn from the $|\Phi|^2$ guiding function with ϵ set to 0.01.

Stage	Method	N_d	TJF	F-matrix	Orbitals	N_p	Iterations
1	Hybrid	10^2	✓			139	9
2	Hybrid	10^3	✓	✓		1048	4
3	Hybrid	10^4	✓	✓	✓	15,573	6
4	AD	10^4	✓	✓	✓	15,573	1,000

spectively. We used a value of 0.001 for ϵ in the $|\Phi|^2$ distribution for the LM and BLM sampling. These optimizations were then followed by 1,000 steps of RMSprop. As shown in Figure 16, we find that our hybrid method reaches a converged energy as low or better than that of the standard and blocked LM, and finishing our optimizations with descent provides a substantial improvement in the statistical uncertainty even in this more challenging case.

FNNF

We now turn our attention to a strongly correlated transition state of the the diflurodiazene (FNNF) *cis-trans* isomerization, where we test the hybrid optimization approach on a much larger determinant expansion. The FNNF isomerization can be thought of as a toy model molecule for larger systems such as photoswitches, which have potential uses in molecular machines [89, 90] and high-density memory storage. [91] In addition, FNNF itself is of interest as part of the synthesis of high energy polynitrogen compounds and has been the subject of multiple electronic structure studies.[92–94] Here we focus on its strongly correlated transition state, which is the direct analogue of the out-of-plane TS1 transition state in diazene. [95]

Our treatment of this transition state began by locating its geometry via an (8e,8o) CASSCF optimization in the cc-pVTZ basis using Molpro.[87] At this geometry (given in Appendix C) we then switch over to using BFD pseudopotentials and their corresponding triple zeta basis, [86] in which we use the Dice code [16, 18] to iterate an HCI calculation with 24 electrons distributed in the lowest 50 (8e,8o) CASSCF orbitals until its variational wave function has reached almost 2 million de-

TABLE V. Energies of the transition state of FNNF.

Method	Energy (a.u.)	Uncertainty (a.u.)
Hartree-Fock	-67.112730	
CASSCF	-67.359100	
VMC Stage 1	-68.1017	0.0011
VMC Stage 2	-68.1213	0.0009
VMC Stage 3	-68.1698	0.0006
VMC Stage 4	-68.1750	0.0002

terminants. We then import the first 10,000 of these determinants into our VMC optimization and combine them with TJFs, atom-centered NCJFs, and orbital optimization, which produces an ansatz with over 15,000 variational parameters.

Our VMC optimization proceeds in stages as summarized in Table IV. This begins with TJFs and a 100-determinant ansatz from HCI, with later optimization stages adding more determinants and turning on the optimization of the NCJF and orbital rotation variables. As in styrene, the strategy is to bring the parameters near to their optimal values with the help of the LM and then to perform a final unbiased relaxation via a long run of RMSprop AD. Due to the large number of variational parameters, we incorporate the LM via the hybrid scheme, with the BLM steps employing 2, 2, and 10 blocks during stages 1, 2, and 3, respectively. In stages 1 and 2, we used an initial RMSprop step size of 0.01 for TJFs and CI coefficients before setting it to 0.005 at the beginning of stage 3. For the F-matrix parameters, we began by setting the initial step size to 0.001, but after observing a significant rise and fall of the energy during the RMSprop section of the first hybrid macro iteration in stage 3, we reduced this to 0.0001 and also lowered the TJF and CI step size to 0.0005 for the last 4 macro iterations in that stage. For all steps in stage 4, we maintained the 0.0001 step size for the F-matrix parameters and lowered the initial step size for TJFs and CI coefficients to 0.0002. An initial step size of 0.0001 was used for orbital parameters throughout both stages 3 and 4. The BLM steps used the $|\Phi|^2$ guiding function with a value of 0.01 for ϵ.

The energies resulting from this staged optimization are shown in Table V and Figure 17. Unsurprisingly, stage 3 proved to be the most challenging and expensive stage, as it is where we hope to move all parameters near to their final values in a setting where the traditional LM would face severe memory bottlenecks. As seen in Figure 17, both the AD and BLM steps clearly work to lower the energy during the first two macro iterations of stage 3. In the last four macro iterations of stage 3, however, the energy decreases more slowly and it is less clear, at least when looking at the energetics, whether the BLM steps are still necessary. Instead, their importance is revealed by inspecting the movement of the F-matrix values within the NCJF, an example of which
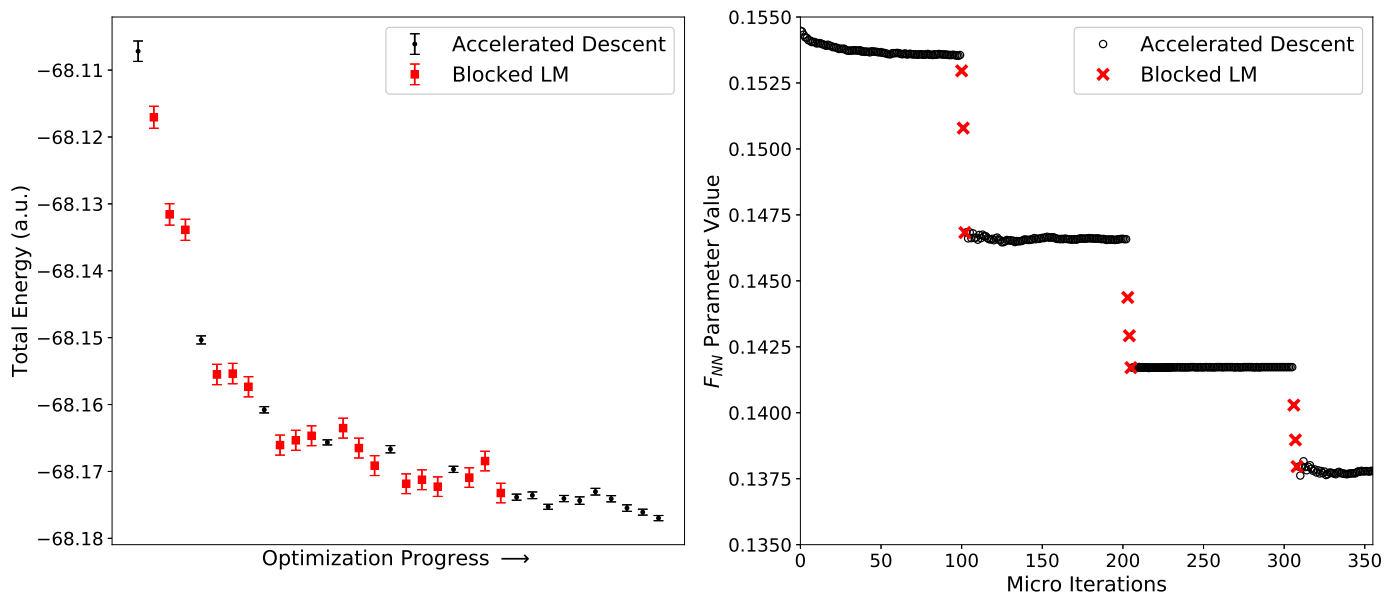
FIG. 17. Left panel: energies during stages 3 and 4 of the FNNF optimization. The descent energies are reported as the average over the last 50 RMSprop steps within each block of 100 RMSprop steps, whereas the BLM energies are the energy estimates on the random samples used for the BLM update steps. Right panel: change in the value of the F-matrix parameter that couples the two nitrogen atoms' counting regions over the first three macro iterations of stage 3, with each micro iteration corresponding to one RMSprop or BLM step. The nine BLM points on the right panel correspond to the first nine BLM points on the left panel.

is shown in the right-hand panel of Figure 17. As in N_2, these parameters prove to be the most resistant to optimization via AD, and we clearly see that although AD does gradually move their values in the same direction as the BLM, the BLM steps dramatically accelerate their optimization. This effect is seen throughout all six macro iterations of stage 3, and so although the BLM energies are not obviously improving at the end of this stage, the inclusion of these steps is clearly still beneficial. Note that relaxing the NCJF after moving from a 1,000-determinant to a 10,000-determinant expansion is important, because the larger determinant expansion is better able to capture some of the correlation effects that the NCJF is encoding, and so we expect (and indeed see) that this diminishing of its role leads to smaller F-matrix values being optimal.

Although we have again found that it would be difficult for AD alone to provide a successful optimization of our ansatz, the statistical advantages of its incorporation are still quite clear. A close inspection of the sample sizes used in the optimization reveals that each of the AD and BLM points in the left panel of Figure 17 corresponds to averaging over 1 million random samples. Despite this equal sampling effort, the uncertainties for the AD energy estimates are about one third the size of those for the BLM, implying that a pure BLM approach would require an order of magnitude more sampling effort to produce similar results. To understand this statistical ad-

vantage, we need to remember two important differences between the AD and BLM steps. First, the nonlinearity of the LM and BLM eigenvalue problem leads to biases in the update steps that can both increase the step-to-step energy uncertainty and cause the method to optimize off-center from the true minimum. Second, the use of an alternative guiding function for the BLM samples in order to mitigate this step uncertainty moves us away from the zero-variance regime enjoyed by traditional $|\Psi|^2$ sampling. If we were to instead employ traditional sampling, our energy estimates for a specific wave function would improve, but the BLM step uncertainty would increase sharply. As the AD methods do not suffer from these issues, they help us to further mitigate the BLM step uncertainty and to perform a final, high-precision relaxation during stage 4. In total, incorporating the AD steps in this case roughly doubles the number of samples required, but is well worthwhile given that it improves statistical efficiency by almost an order of magnitude.

While it is possible that the NCJF parameters are not quite converged in this particular optimization and that increasing iteration counts in stages 1 through 3 could further improve the energy, the lessons learned from investigating a large MSJ optimization for the FNNF transition state are already clear. While both the BLM and the AD methods can be used in this 10,000+ parameter regime, they bring highly complementary advantages to the optimization and so would appear to work better to-

gether than apart. In particular, the BLM helps optimize the parameters that change only very slowly during AD, whereas the statistical advantages of AD greatly increase precision at a given sample size and work to eliminate the statistical biases suffered by the BLM.

CONCLUSIONS AND OUTLOOK

We have found that a combination of first and second derivative optimization methods appears to work better than using either class of method on its own when minimizing the energies of wave functions in variational Monte Carlo. This is particularly true for wave functions with a wide variety of different types of nonlinear parameters, as for example when dealing simultaneously with traditional one- and two-body Jastrow factors, many-body Jastrow factors, and orbital relaxations. While the linear method and its low-memory variants show a superior ability to move these nonlinear parameters into the vicinity of their optimal values, accelerated descent methods prove much more capable of converging them tightly around the minimum. This situation stands as an interesting reverse of what is typically encountered in deterministic optimization, where second derivative methods are usually superior for tight final convergence and first derivative methods perform relatively better in the early stages of an optimization. The realities of working with statistically uncertain energies and energy derivatives turns this expectation on its head, both because of the need to stabilize the statistics of the linear method's second derivative elements through zero-variance-violating importance sampling schemes and due to the nonlinear biases that are induced when solving the linear method's eigenvalue problem. The linear method's ability to quickly move the parameters near the minimum, however, makes it appear that employing it as part of a hybrid approach is well worthwhile. Indeed, in our testing, hybridizing low-memory linear method variants with accelerated descent methods provides better energies with smaller statistical uncertainties at a lower computational cost when compared to the stand-alone use of either the linear method or accelerated descent methods.

Looking forward, there are many questions still to be answered about the interplay between first and second derivative methods. For example, although the blocked linear method greatly reduces memory cost vs the traditional linear method, it is not clear that it can be applied effectively beyond 100,000 parameters in its current form. One thus wonders whether it is necessary to optimize all of the parameters during the linear method steps of the hybrid approach, or whether it may be possible to identify (perhaps during an ongoing optimization?) which parameters would benefit from linear method treatment and which would not. Were such a sorting possible, accelerated descent methods with their even lower memory footprint could be left to deal with most of the parameters, with only a relatively small subset treated by the linear method steps. Another important issue is making the hybrid approach as black box and user friendly as possible. Although we have tested it here with many different descent step size settings for the different parameter types, this has not been a systematic survey. More extensive testing may allow clear defaults to be settled upon so that users can reasonably expect a successful optimization without resorting to careful step size control. We look forward to investigating these exciting possibilities in future.

ACKNOWLEDGEMENTS

APPENDIX A: ADDITIONAL ENERGIES

TABLE VI. Precise Values for optimizing CI coefficients and traditional Jastrow factors in equilibrium N_2.

Method	Energy (a.u.)	Uncertainty (a.u.)	Samples
Hybrid 1	-19.9083	0.0005	3,900,000
Hybrid 2	-19.9095	0.0006	5,400,000
Hybrid 3	-19.9101	0.0005	29,000,000
RMSprop 1	-19.8936	0.0006	20,000,000
RMSprop 2	-19.9091	0.0005	20,000,000
AMSGrad 1	-19.8998	0.0007	20,000,000
AMSGrad 2	-19.8926	0.0008	20,000,000
AMSGrad 3	-19.9048	0.0006	20,000,000
AMSGrad 4	-19.9071	0.0005	20,000,000
ADAM 1	-19.9009	0.0005	20,000,000
ADAM 2	-19.9056	0.0006	20,000,000
ADAM 3	-19.9078	0.0005	20,000,000
Random 1	-19.8926	0.0006	20,000,000
Random 2	-19.9041	0.0005	20,000,000
Linear Method	-19.9105	0.0010	40,000,000

TABLE VII. Precise Values for optimizing CI coefficients and traditional Jastrow factors in stretched N_2.

Method	Energy (a.u.)	Uncertainty (a.u.)	Samples
Hybrid 1	-19.6141	0.0005	27,000,0000
RMSprop 1	-19.6010	0.0007	20,000,000
RMSprop 2	-19.6137	0.0005	20,000,000
AMSGrad 1	-19.6044	0.0006	20,000,000
AMSGrad 2	-19.5858	0.0007	20,000,000
AMSGrad 3	-19.6096	0.0006	20,000,000
ADAM 1	-19.6028	0.0006	20,000,000
ADAM 2	-19.6105	0.0005	20,000,000
Random 1	-19.5937	0.0006	20,000,000
Random 2	-19.6147	0.0006	20,000,000
Linear Method	-19.6155	0.0010	40,000,000

APPENDIX B: DETAILS FOR N_2 OPTIMIZATIONS

The details for the optimizations behind the final energies in the main paper are presented below. In every case of N_2, all flavors of pure gradient descent based optimization were run for 2000 iterations at 10,000 samples per iteration except for the random step size method, which was run for 10,000 iterations at 2000 samples per iteration. The total sampling cost was then 20 million samples, half of the standard linear method's cost of 40 million over 40 steps. Given the descent methods' tendency to plateau after a few hundred iterations and then lower the energy by only a few mE_h afterward, we expect that running them longer to fully match or exceed the linear method's sampling effort would not yield a much better result in most cases. We found that it was often advantageous to allow for different types of parameters to be given different initial step sizes. Tables VIII through XI list the step sizes for different descent optimizations in all cases of N_2. The values can be cross-referenced with the energy results in earlier tables to see which choices were most effective. Some amount of experimentation was necessary to build up intuition for what choices are effective, but we generally expect more nonlinear parameters such as those in the F-matrix and the orbitals to require smaller step sizes. We also found that RMSprop benefited from using larger step sizes compared to other descent algorithms. The energy may be significantly raised on early iterations, but tends to be quickly lowered and eventually brought to an improved result once enough gradient history has built up over more steps.

The details of the different hybrid method optimizations are slightly more involved and are discussed separately here. In all cases, the blocked linear method steps of the hybrid optimization used 5 blocks with 5 directions from sections of RMSprop to provide coupling to variables outside a block and retained 30 directions from each block to construct the final space for determining the parameter update. These were also the settings given to the blocked linear method optimizations of N_2 that appear in the main text. All hybrid optimizations used the RMSprop method for their AD sections with the hyperparameters $d = 100$, $\rho = .9$ and $\epsilon = 10^{-8}$. The step sizes used in the AD sections varied over the course of the hybrid optimizations. We typically chose larger step sizes for the AD portion of the first macro-iteration in order to obtain more energy and parameter improvement at a low sampling cost before any use of the BLM and these are tabulated separately as "Hybrid-Initial". The smaller step sizes reported for the rest of hybrid optimization were used in the later macro-iterations to avoid rises in the energy that might occur before a sufficient gradient history was accumulated. We also list the step sizes in the long RMSprop optimization used to achieve the descent finalized energies. These were sometimes larger than those for the AD sections of the initial hybrid optimizations because the descent finalization was long enough for any early transient rises in the energy to recover.

We now specify how the hybrid method sampling costs reported in Tables II and III of the main paper were divided between AD and the BLM. In all parameter equilibrium N_2, Hybrid 1 consisted of 500 AD steps costing 3 million samples interwoven with 12 BLM steps that cost 2.4 million samples. Hybrid 2 consisted of the same sequence of steps, but had an increased sampling effort of 6 million samples on descent and 2.4 million on BLM. Hybrid 3 had a greatly increased sampling cost and consisted of 1400 AD steps for 11.2 million samples interwoven with 19 BLM steps costing 38 million. For all parameter stretched N_2, Hybrid 1 used the same sequence of steps and sampling cost breakdown as Hybrid 1 for the equilibrium case. Hybrid 2 consisted of 600 AD steps that cost 7 million samples and 15 BLM steps that cost 3 million. Hybrid 3 also had 600 AD steps, now using 12 million samples, and 15 BLM steps, now using 30 million samples. For all descent finalizations in N_2, we used 1000 steps of RMSprop at an additional cost of 10 million samples and took an average over the last 500 steps to obtain our reported energies and error bars.

Finally, we give the breakdown of the hybrid sampling costs in Tables VI and VII of Appendix A. For the equilibrium case, Hybrid 1 had 500 AD steps costing 1.5 million samples and 12 BLM steps costing 2.4 million samples. Hybrid 2 had the same combination of steps and BLM cost as Hybrid 1 while the AD steps used 3 million samples. Hybrid 3 used the same sequence of steps, but increased the AD and BLM sampling costs to 5 million and 24 million, respectively. In the stretched case, the hybrid optimization used 500 AD steps with 3 million samples and 12 BLM steps costing 24 million samples.

TABLE VIII. Step sizes for TJFCI equilibrium N_2 optimizations.

Method	2-Body TJF	1-Body TJF	CI
RMSprop 1	0.01	0.01	0.005
RMSprop 2	0.05	0.05	0.01
AMSGrad 1	0.05	0.05	0.01
AMSGrad 2	0.05	0.05	0.05
AMSGrad 3	0.01	0.01	0.01
AMSGrad 4	0.001	0.001	0.001
ADAM 1	0.01	0.01	0.01
ADAM 2	0.005	0.005	0.005
ADAM 3	0.001	0.001	0.001
Random 1	0.01	0.01	0.01
Random 2	0.0005	0.0005	0.0005
Hybrid-Initial 1	0.1	0.1	0.01
Hybrid-Initial 2	0.1	0.1	0.01
Hybrid-Initial 3	0.1	0.1	0.01
Hybrid 1	0.001	0.001	0.001
Hybrid 2	0.005	0.005	0.005
Hybrid 3	0.005	0.005	0.005

TABLE IX. Step sizes for TJFCI stretched N_2 optimizations.

Method	2-Body TJF	1-Body TJF	CI
RMSprop 1	0.01	0.01	0.005
RMSprop 2	0.05	0.05	0.01
AMSGrad 1	0.05	0.05	0.01
AMSGrad 2	0.05	0.05	0.05
AMSGrad 3	0.01	0.01	0.01
ADAM 1	0.01	0.01	0.01
ADAM 2	0.005	0.005	0.005
Random 1	0.01	0.01	0.01
Random 2	0.001	0.001	0.001
Hybrid-Initial 1	0.1	0.1	0.1
Hybrid 1	0.005	0.005	0.005

TABLE X. Step sizes for all parameter equilibrium N_2 optimizations.

Method	2-Body TJF	1-Body TJF	F-Matrix	CI	Orbitals
RMSprop 1	0.005	0.005	0.001	0.001	0.001
RMSprop 2	0.05	0.05	0.01	0.01	0.01
AMSGrad 1	0.05	0.05	0.005	0.01	0.001
AMSGrad 2	0.005	0.005	0.001	0.001	0.001
ADAM 1	0.05	0.05	0.005	0.01	0.001
ADAM 2	0.005	0.005	0.001	0.001	0.001
Random 1	0.001	0.001	0.001	0.001	0.001
Random 2	0.001	0.001	0.0005	0.001	0.0005
Hybrid-Initial 1	0.1	0.1	0.0001	0.01	0.01
Hybrid-Initial 2	0.1	0.1	0.0005	0.01	0.01
Hybrid-Initial 3	0.01	0.01	0.001	0.01	0.001
Hybrid 1	0.0001	0.0001	0.0001	0.0001	0.0001
Hybrid 2	0.001	0.001	0.0005	0.0005	0.0005
Hybrid 3	0.001	0.001	0.001	0.001	0.001
DF-Hybrid 1	0.001	0.001	0.001	0.001	0.001
DF-Hybrid 2	0.001	0.001	0.001	0.001	0.001
DF-Hybrid 3	0.001	0.001	0.001	0.001	0.001

TABLE XI. Step sizes for all parameter stretched N_2 optimizations.

Method	2-Body TJF	1-Body TJF	F-Matrix	CI	Orbitals
RMSprop 1	0.05	0.05	0.05	0.01	0.01
RMSprop 2	0.1	0.1	0.01	0.01	0.005
AMSGrad 1	0.05	0.05	0.05	0.01	0.01
AMSGrad 2	0.05	0.05	0.01	0.02	0.001
AMSGrad 3	0.005	0.005	0.001	0.002	0.001
ADAM 1	0.05	0.05	0.05	0.01	0.01
ADAM 2	0.05	0.05	0.01	0.02	0.001
ADAM 3	0.005	0.005	0.001	0.002	0.001
Random 1	0.001	0.001	0.001	0.001	0.001
Random 2	0.001	0.001	0.0005	0.001	0.0005
Hybrid-Initial 1	0.1	0.1	0.01	0.01	0.001
Hybrid-Initial 2	0.1	0.1	0.01	0.01	0.001
Hybrid-Initial 3	0.1	0.1	0.01	0.01	0.001
Hybrid 1	0.0001	0.0001	0.0001	0.0001	0.0001
Hybrid 2	0.001	0.001	0.0005	0.0005	0.0005
Hybrid 3	0.001	0.001	0.0005	0.0005	0.0005
DF-Hybrid 1	0.001	0.001	0.001	0.001	0.001
DF-Hybrid 2	0.001	0.001	0.001	0.001	0.001
DF-Hybrid 3	0.001	0.001	0.001	0.001	0.001

APPENDIX C: MOLECULAR GEOMETRIES

TABLE XII. Structure of equilibrium styrene. Coordinates in Å.

C	1.39295	0.00000	0.00000
C	2.16042	-1.19258	0.01801
C	2.09421	1.23178	-0.01914
C	3.56585	-1.15969	0.05286
C	3.50142	1.27211	0.01795
C	4.23686	0.07503	0.06081
C	0.00000	0.00000	0.00000
C	-0.79515	-0.93087	0.54406
H	1.71222	-2.11161	-0.00239
H	1.59237	2.12471	-0.04753
H	4.09818	-2.03273	0.07153
H	3.99086	2.16987	0.01692
H	5.25794	0.10043	0.09503
H	-0.46324	0.77112	-0.42775
H	-0.43431	-1.72147	1.02278
H	-1.78240	-0.84577	0.49296

TABLE XIII. Structure of FNNF transition state. Coordinates in Å.

N	0.49939	-0.44656	-0.59377
N	0.57066	0.41224	0.5639
F	-0.39084	0.14563	-1.36959
F	-0.39807	-0.12032	1.39157

APPENDIX D: NCJF GAUSSIAN BASIS

The form for the three dimensional Gaussian basis functions of NCJFs in the main text can equivalently be written as $g_j(\mathbf{r}) = \exp(\mathbf{r}^T \mathbf{A} \mathbf{r} - 2\mathbf{B}^T \mathbf{r} + C)$ where $\mathbf{A}$ is a symmetric matrix defined by 6 parameters, $\mathbf{B}$ is a three-component vector, and C is a single dimensionless number. We used 16 basis functions for the all parameter cases of N_2, 16 in styrene, and 4 in FNNF. Their complete specifications are presented in Tables XIV-XVIII. The components $A_{xx}, A_{xy}, A_{xz}, A_{yy}, A_{yz}, A_{zz}$ with units of inverse square bohr are the same for each basis function within a particular system and are therefore listed separately in Table XIV. Tables XV-XVIII contain components B_x, B_y, B_z, with units of inverse bohr and C for each system's basis functions.

TABLE XIV. Components of the matrix $\mathbf{A}$ for our systems.

System	A_{xx}	A_{xy}	A_{xz}	A_{yy}	A_{yz}	A_{zz}
Equilibrium N_2	-6.9282	0.0	0.0	-6.9282	0.0	-6.9282
Stretched N_2	-6.9282	0.0	0.0	-6.9282	0.0	-6.9282
Styrene	-0.1	0.0	0.0	-0.1	0.0	-0.1
FNNF	-0.1	0.0	0.0	-0.1	0.0	-0.1

TABLE XV. Gaussian components for all parameter equilibrium N_2.

Basis Function	B_x	B_y	B_z	C
g_0	-0.8	-0.8	-0.8	-0.2771
g_1	0.8	-0.8	-0.8	-0.2771
g_2	-0.8	0.8	-0.8	-0.2771
g_3	0.8	0.8	-0.8	-0.2771
g_4	-0.8	-0.8	0.8	-0.2771
g_5	0.8	-0.8	0.8	-0.2771
g_6	-0.8	0.8	0.8	-0.2771
g_7	0.8	0.8	0.8	-0.2771
g_8	-4.4787	-0.8	-0.8	-11.2500
g_9	-2.8787	-0.8	-0.8	-4.5981
g_{10}	-4.4787	0.8	-0.8	-11.2500
g_{11}	-2.8787	0.8	-0.8	-4.5981
g_{12}	-4.4787	-0.8	0.8	-11.2500
g_{13}	-2.8787	-0.8	0.8	-4.5981
g_{14}	-4.4787	0.8	0.8	-11.2500
g_{15}	-2.8787	0.8	0.8	-4.5981

TABLE XVI. Gaussian basis functions for all parameter stretched N_2.

Basis Function	B_x	B_y	B_z	C
g_0	-0.8	-0.8	-0.8	-0.2771
g_1	0.8	-0.8	-0.8	-0.2771
g_2	0.8	0.8	-0.8	-0.2771
g_3	0.8	0.8	-0.8	-0.2771
g_4	-0.8	-0.8	0.8	-0.2771
g_5	0.8	-0.8	0.8	-0.2771
g_6	-0.8	0.8	0.8	-0.2771
g_7	0.8	0.8	0.8	-0.2771
g_8	-5.8015	-0.8	-0.8	-22.7322
g_9	-4.2015	-0.8	-0.8	-11.8474
g_{10}	-5.8015	0.8	-0.8	-22.7322
g_{11}	-4.2015	0.8	-0.8	-11.8474
g_{12}	-5.8015	-0.8	0.8	-22.7322
g_{13}	-4.2015	-0.8	0.8	-11.8474
g_{14}	-5.8015	0.8	0.8	-22.7322
g_{15}	-4.2015	0.8	0.8	-11.8474

TABLE XVII. Gaussian basis functions for equilibrium styrene.

Basis Function	B_x	B_y	B_z	C
g_0	-0.2632	0.0	0.0	-0.6929
g_1	-0.4083	0.2254	-0.003403	-2.1748
g_2	-0.3957	-0.2328	0.003617	-2.1081
g_3	-0.6738	0.2191	-0.009989	-5.0220
g_4	-0.6617	-0.2404	-0.003392	-4.9561
g_5	-0.8007	-0.01418	-0.01149	-6.4137
g_6	0.0	0.0	0.0	0.0
g_7	0.1503	0.1759	-0.1028	-0.6409
g_8	-0.3236	0.3990	0.0004516	-2.6392
g_9	-0.3009	-0.4015	0.008982	-2.5184
g_{10}	-0.7744	0.3841	-0.01352	-7.4750
g_{11}	-0.7542	-0.41005	-0.003197	-7.3691
g_{12}	-0.9936	-0.01898	-0.01796	-9.8794
g_{13}	0.08754	-0.1457	0.08083	-0.3543
g_{14}	0.08207	0.3253	-0.19328	-1.4992
g_{15}	0.3368	0.1598	-0.09316	-1.4767

TABLE XVIII. Gaussian basis functions for FNNF.

Basis Function	B_x	B_y	B_z	C
g_0	-0.09437	0.08439	0.1122	-0.2862
g_1	-0.1078	-0.07790	-0.1066	-0.2905
g_2	0.07386	-0.02752	0.2588	-0.7320
g_3	0.07522	0.02274	-0.2630	-0.7533

* eneuscamman@berkeley.edu

[1] P. Pulay, J. Comput. Chem. **3**, 556 (1982).
[2] E. R. Davidson, J. Comput. Phys **17**, 87 (1975).
[3] S. R. White, Phys. Rev. B **72**, 180403 (2005).
[4] C. J. Umrigar, J. Toulouse, C. Filippi, S. Sorella, and R. G. Hennig, Phys. Rev. Lett. **98**, 110201 (2007).
[5] E. Neuscamman, C. J. Umrigar, and G. K. L. Chan, Phys. Rev. B. **85**, 045103 (2012).
[6] L. Zhao and E. Neuscamman, J. Chem. Theory Comput. **13**, 2604 (2017).
[7] L. R. Schwarz, A. Alavi, and G. H. Booth, Phys. Rev. Lett. **118**, 176403 (2017).
[8] I. Sabzevari and S. Sharma, J. Chem. Theory Comput. **14**, 6276 (2018).
[9] A. Mahajan and S. Sharma, arXiv.org , 1902.07690 (2019).
[10] D. Luo and B. K. Clark, arXiv.org , 1807.10770 (2018).
[11] B. K. Clark, M. A. Morales, J. McMinis, J. Kim, and G. E. Scuseria, J. Chem. Phys. **135**, 244105 (2011).
[12] M. A. Morales, J. McMinis, B. K. Clark, J. Kim, and G. E. Scuseria, J. Chem. Theory Comput. **8**, 2181 (2012).
[13] C. Filippi, R. Assaraf, and S. Moroni, J. Chem. Phys. **144**, 194105 (2016).
[14] R. Assaraf, S. Moroni, and C. Filippi, J. Chem. Theory Comput. **13**, 5273 (2017), 1706.07588.
[15] J. Schriber and F. Evangelista, J. Chem. Phys. **144**, 161106 (2016).
[16] A. A. Holmes, N. M. Tubman, and C. J. Umrigar, J. Chem. Theory Comput. **12**, 3674 (2016).
[17] N. M. Tubman, J. Lee, T. Y. Takeshita, M. Head-Gordon, and K. B. Whaley, J. Chem. Phys. **145**, 044112 (2016).
[18] S. Sharma, A. A. Holmes, G. Jeanmairet, A. Alavi, and C. J. Umrigar, J. Chem. Theory Comput. **13**, 1595 (2017).
[19] Y. Garniron, A. Scemama, E. Giner, M. Caffarel, and P.-F. Loos, J. Chem. Phys. **149**, 064103 (2018).
[20] A. D. Chien, A. A. Holmes, M. Otten, C. J. Umrigar, S. Sharma, and P. M. Zimmerman, J. Phys. Chem. A **122**, 2714 (2018).
[21] H. J. Changlani, J. M. Kinder, C. J. Umrigar, and G. K.-L. Chan, Phys. Rev. B **80**, 245116 (2009).
[22] F. Mezzacapo, N. Schuch, M. Boninsegni, and J. I. Cirac, New J. Phys. **11**, 083026 (2009).
[23] E. Neuscamman and G. K.-L. Chan, Phys. Rev. B **86**, 064402 (2012).
[24] M. Casula, C. Attaccalite, and S. Sorella, J. Chem. Phys. **121**, 7110 (2004).
[25] S. Sorella, M. Casula, and D. Rocca, J. Chem. Phys. **127**, 014105 (2007).
[26] P. López Ríos, P. Seth, N. D. Drummond, and R. J. Needs, Phys. Rev. E. **86**, 036703 (2012).
[27] A. Lüchow, A. Sturm, C. Schulte, and K. Haghighi Mood, J. Chem. Phys. **142**, 084111 (2015).
[28] B. V. D. Goetz and E. Neuscamman, J. Chem. Theory Comput. **13**, 2035 (2017).
[29] B. V. D. Goetz, L. Otis, and E. Neuscamman, J. Chem. Theory Comput. **15**, 1102 (2018).
[30] M. Taddei, M. Ruggeri, S. Moroni, and M. Holzmann, Phys. Rev. B **91**, 115106 (2015).
[31] L. Zhao and E. Neuscamman, J. Chem. Theory Comput. **12**, 3436 (2016).
[32] E. Neuscamman, J. Chem. Phys. **145**, 081103 (2016).
[33] N. S. Blunt and E. Neuscamman, J. Chem. Phys. **147**, 194101 (2017).
[34] J. A. R. Shea and E. Neuscamman, J. Chem. Theory Comput. **13**, 6078 (2017).
[35] P. J. Robinson, S. D. Pineda Flores, and E. Neuscamman, J. Chem. Phys. **147**, 164114 (2017).
[36] N. S. Blunt and E. Neuscamman, J. Chem. Theory Comput. **15**, 178 (2018).
[37] S. D. P. Flores and E. Neuscamman, J. Phys. Chem. A **123**, 1487 (2019).
[38] G. Carleo and M. Troyer, Science **355**, 602 (2017).
[39] D. Kochkov and B. K. Clark, arXiv.org , 1811.12423 (2018).
[40] E. Neuscamman, J. Chem. Theory Comput. **12**, 3149 (2016), 1603.06605.
[41] W. M. C. Foulkes, L. Mitas, R. J. Needs, and G. Rajagopal, Rev. Mod. Phys. **73**, 33 (2001).
[42] S. Zhang, F. D. Malone, and M. A. Morales, J. Chem. Phys. **149**, 164102 (2018).
[43] L. Zhao and E. Neuscamman, arXiv.org , 1804.09663 (2018).
[44] C. J. Umrigar, J. Chem. Phys. **143**, 164105 (2015).
[45] R. Assaraf and M. Caffarel, Physical Review Letters **83**, 4682 (1999).
[46] J. R. Trail, Phys. Rev. E. **77**, 016703 (2008).
[47] J. R. Trail, Phys. Rev. E. **77**, 016704 (2008).
[48] T. Helgaker, P. Jorgensen, and J. Olsen, *Molecular Electronic-Structure Theory* (John Wiley & Sons, Chichester, 2000).
[49] A. Harju, B. Barbiellini, S. Siljamäki, R. M. Nieminen, and G. Ortiz, Phys. Rev. Lett. **79**, 1173 (1997).
[50] X. Lin, H. Zhang, and A. M. Rappe, J. Chem. Phys. **112**, 2650 (2000).
[51] M. W. Lee, M. Mella, and A. M. Rappe, J. Chem. Phys. **122**, 244103 (2005).
[52] S. Sorella, Phys. Rev. B **71**, 241103 (2005).
[53] C. J. Umrigar and C. Filippi, Phys. Rev. Lett. **94**, 150201 (2005).
[54] P. R. C. Kent, R. J. Needs, and G. Rajagopal, Phys. Rev. B. **59**, 12344 (1999).
[55] C. J. Umrigar, K. G. Wilson, and J. W. Wilkins, Phys. Rev. Lett. **60**, 1719 (1988).
[56] M. P. Nightingale and V. Melik-Alaverdian, Phys. Rev. Lett. **87**, 43401 (2001).
[57] J. Toulouse and C. J. Umrigar, J. Chem. Phys. **126**, 084102 (2007).
[58] J. Kim, A. Baczewski, T. D. Beaudet, A. Benali, M. C. Bennett, M. A. Berrill, N. S. Blunt, E. J. L. Borda, M. Casula, D. M. Ceperley, B. K. Clark, R. C. C. Iii, K. T. Delaney, M. Dewing, K. P. Esler, H. Hao, O. Heinonen, P. R. C. Kent, J. T. Krogel, I. Kylan-

paa, Y. W. Li, M. G. Lopez, Y. Luo, F. D. Malone, R. M. Martin, A. Mathuriya, J. Mcminis, C. A. Melton, L. Mitas, M. A. Morales, E. Neuscamman, W. D. Parker, S. D. P. Flores, N. A. Romero, B. M. Rubenstein, J. A. R. Shea, H. Shin, L. Shulenburger, A. Tillack, J. P. Townsend, N. M. Tubman, B. Van Der Goetz, J. E. Vincent, D. C. Yang, Y. Yang, S. Zhang, and L. Zhao, J. Phys. Condens. Matter **30**, 195901 (2018).

[59] J. Toulouse and C. J. Umrigar, J. Chem. Phys. **128**, 174101 (2008).

[60] M. D. Brown, J. R. Trail, P. L. Ríos, and R. J. Needs, J. Chem. Phys. **126**, 224110 (2007), 1011.4343.

[61] F. R. Petruzielo, J. Toulouse, and C. J. Umrigar, J. Chem. Phys. **136**, 124116 (2012).

[62] L. Zhao and E. Neuscamman, J. Chem. Theory Comput. **12**, 3719 (2016).

[63] N. S. Blunt, A. Alavi, and G. H. Booth, Phys. Rev. B. **98**, 085118 (2018).

[64] L. R. Schwarz, *Projector Quantum Monte Carlo Methods for Linear and Non-linear Wavefunction Ansatzes*, Ph.D. thesis, University of Cambridge (2017).

[65] J. H. Choi and C. F. Lebeda, Chem. Phys. Lett. **5**, 503 (1970).

[66] H. Z. Ye, M. Welborn, N. D. Ricke, and T. Van Voorhis, J. Chem. Phys. **147**, 214104 (2017).

[67] L. Bottou, "Stochastic gradient descent tricks," in *Neural Networks, Tricks of the Trade*, Lecture Notes in Computer Science (LNCS) (Springer, 2012) pp. 430–445, neural networks: tricks of the trade, 2nd ed.

[68] D. Kingma and J. Ba, arXiv.org , 1412.6980 (2014).

[69] S. Ruder, arXiv.org , 1609.04747 (2016).

[70] S. J. Reddi, S. Kale, and S. Kumar, International Conference on Learning Representations , 1 (2018).

[71] C. J. Huang, C. J. Umrigar, and M. P. Nightingale, J. Chem. Phys. **107**, 3007 (1997).

[72] M. Casula and S. Sorella, J. Chem. Phys. **119**, 6500 (2003).

[73] T. D. Beaudet, M. Casula, J. Kim, S. Sorella, and R. M. Martin, J. Chem. Phys. **129**, 164711 (2008).

[74] F. Sterpone, L. Spanu, L. Ferraro, S. Sorella, and L. Guidoni, J. Chem. Theory Comput. **4**, 1428 (2008).

[75] M. Marchi, S. Azadi, M. Casula, and S. Sorella, J. Chem. Phys. **131**, 154116 (2009).

[76] M. Barborini, S. Sorella, and L. Guidoni, J. Chem. Theory Comput. **8**, 1260 (2012).

[77] A. Zen, Y. Luo, G. Mazzola, L. Guidoni, and S. Sorella, J. Chem. Phys. **142**, 144111 (2015).

[78] M. C. Gutzwiller, Phys. Rev. **137**, A1726 (1965).

[79] E. Neuscamman, J. Chem. Phys. **139**, 181101 (2013).

[80] S. R. Langhoff and E. R. Davidson, Int. J. Quantum Chem. **VIII**, 61 (1974).

[81] E. Rossi, G. L. Bendazzoli, S. Evangelisti, and D. Maynau, Chem. Phys. Lett. **310**, 530 (1999).

[82] G. K. L. Chan, M. Kállay, and J. Gauss, J. Chem. Phys. **121**, 6110 (2004).

[83] B. Braïda, J. Toulouse, M. Caffarel, and C. J. Umrigar, J. Chem. Phys. **134**, 084108 (2011).

[84] D. A. Mazziotti, Phys. Rev. Lett. **93**, 213001 (2004).

[85] K. K. Baldridge, J. A. Boatz, S. T. Elbert, M. S. Gordon, J. H. Jensen, S. Koseki, N. Matsunaga, K. A. Nguyen, S. SU, T. Windus, M. Dupuis, and J. A. Montgomery, J. Comput. Chem **14**, 1347 (1993).

[86] M. Burkatzki, C. Filippi, and M. Dolg, J. Chem. Phys. **126**, 234105 (2007).

[87] H.-J. Werner, P. J. Knowles, G. Knizia, F. R. Manby, M. Schütz, *et al.*, "Molpro, version 2019.1, a package of ab initio programs," (2019), see http://www.molpro.net.

[88] M. C. Bennett, C. A. Melton, A. Annaberdiyev, G. Wang, L. Shulenburger, and L. Mitas, J. Chem. Phys. **147**, 224106 (2017).

[89] M. M. Russew and S. Hecht, Adv. Mater. **22**, 3348 (2010).

[90] K. Kinbara and T. Aida, Chem. Rev. **105**, 1377 (2005).

[91] H. Tian and S. Yang, Chem. Soc. Rev. **33**, 85 (2004).

[92] K. O. Christe, R. D. Wilson, W. W. Wilson, R. Bau, S. Sukumar, and D. A. Dixon, Inorg. Chem. **113**, 3795 (1991).

[93] K. O. Christe, D. A. Dixon, D. J. Grant, R. Haiges, F. S. Tham, A. Vij, V. Vij, T. H. Wang, and W. W. Wilson, Inorg. Chem. **49**, 6823 (2010).

[94] T. J. Lee, J. E. Rice, G. E. Scuseria, and H. F. Schaefer, Theor. Chim. Acta **75**, 81 (1989).

[95] A. M. Sand, C. A. Schwerdtfeger, and D. A. Mazziotti, J. Chem. Phys. **136**, 034112 (2012).